Advancing Nanocarriers for Targeted Anticancer Drug Delivery using DFT and Docking Simulations of Coronene Nanosheet Interactions

Submitted By

Md. Safayat Hossain
Student ID: IT 20005
Session:2019-20

Anik Adnan
ID: IT-20021
Session: 2019-20

Supervised By

Dr. Mohammad Badrul Alam Miah
Professor

A thesis submitted in partial fulfillment of the requirements for the degree of Bachelor of Science (Engg.) in Information and Communication Technology

Department of Information and Communication Technology
Mawlana Bhashani Science and Technology University
Santosh, Tangail-1902, Bangladesh
May 2025

Supervisor Declaration

I hereby declare that the thesis report titled "**Advancing Nanocarriers for Targeted Anticancer Drug Delivery using DFT and Docking Simulations of Coronene Nanosheet Interactions**" is submitted by Md. Safayat Hossain and Anik Adnan, students of the Department of Information and Communication Technology, Mawlana Bhashani Science and Technology University, have conducted research under my supervision. I have reviewed the work and am satisfied that it meets the standards required for the degree.

Dr. Mohammad Badrul Alam Miah
Professor
Department of ICT, MBSTU
Santosh, Tangail-1902, Dhaka, Bangladesh

.....
Signature of Supervisor

Student Declaration

I hereby declare that this work, titled, *"***Advancing Nanocarriers for Targeted Anticancer Drug Delivery using DFT and Docking Simulations of Coronene Nanosheet Interactions***"* is our thesis and confirm that any part of this thesis has not been submitted or accepted for any degree or any other qualification at this university or any other institution.

Md. Safayat Hossain

Department of ICT, MBSTU .....

Santosh, Tangail-1902, Dhaka, Bangladesh Signature of Candidate

Anik Adnan

Department of ICT, MBSTU .....

Santosh, Tangail-1902, Dhaka, Bangladesh Signature of Candidate

Approval

This is to certify that the thesis work submitted by Md. Safayat Hossain(IT-20005) and Anik Adnan(IT-20021), titled **"Advancing Nanocarriers for Targeted Anticancer Drug Delivery using DFT and Docking Simulations of Coronene Nanosheet Interactions"** has been approved by the examination committee for the partial fulfillment of the requirements for the degree of Bachelor of Science (Engg.) in the Department of Information and Communication Technology, Mawlana Bhashani Science and Technology University, Santosh, Tangail-1902, Bangladesh in December 2022.

Examination Committee

Dr. Mohammad Badrul Alam Miah Professor Department of ICT, MBSTU Santosh, Tangail-1902, Dhaka, Bangladesh	..... Signature of Chairman
Dr. Monir Morshed Professor Department of ICT,MBSTU Santosh,Tangail-1902,Dhaka, Bangladesh	..... Signature of Member (Internal)
Mr. Mehedi Hasan lecturer Department of ICT, MBSTU Santosh, Tangail-1902, Dhaka, Bangladesh	..... Signature of Member (Internal)
Dr. M Shamim Kaisar Professor Department of IIT, JU Savar, Dhaka, Bangladesh	..... Signature of Member (External)

Acknowledgments

First of all, we are grateful to the Almighty Creator for granting us the ability to reach this stage and for His eternal blessings. God has truly blessed us with everything one could hope for.

We would like to express our deepest gratitude and profound respect to our honorable supervisor, Dr. Mohammad Badrul Alam Miah, Professor, Department of Information and Communication Technology, Mawlana Bhashani Science and Technology University (MBSTU), for his continuous support, kind guidance, and constructive feedback throughout the course of our research. Without his patience, encouragement, and valuable insights, this thesis would not have been possible.

We are also sincerely thankful to our honorable teachers Prof. Dr. Sajjad Waheed; Prof. Dr. Monir Morshed, Chairman; Prof. Dr. Muhammad Shahin Uddin; Prof. Dr. Mst. Nargis Aktar; Dr. Md. Abir Hossain, Associate Professor; Dr. Ziaur Rahman, Associate Professor; Mr.Nazrul Islam, Associate Professor; Mr. Mehedi Hassan, Lecturer; and Md. Anowar Kabir, Lecturer for their invaluable suggestions and continuous inspiration during our academic journey.

Finally, our heartfelt thanks go to all the members of the Department of Information and Communication Technology, MBSTU, for creating a supportive academic environment that enabled our work.

Last but not least, we would like to extend our warmest gratitude to our families and friends for their constant love, motivation, and unwavering support throughout this endeavor. Without their encouragement and understanding, this thesis would not have been possible.

Abstract

Cancer continues to be among the top causes of mortality across the globe, highlighting the critical demand for innovative and effective treatment solutions. A potential pathway for progress lies in the use of nanotechnology for drug delivery, which provides considerable improvements by allowing more accurate targeting and supporting the simultaneous delivery of various alternative therapies in cancer care. In this research, we investigated the interactions of several cancer-fighting drugs 5-FU, 6-TG, and 6-MP with both pristine and specially modified coronene nanosheets. Utilizing Density Functional Theory (DFT), we evaluated the effectiveness of four different modified versions in improving drug loading, solubility, and electrostatic interactions: $C_{12}H_{12}B_6N_6$, $H_{12}B_{12}N_{12}$, $C_{12}H_8B_6N_6P_4$, $B_{12}N_{12}P_{12}$, $C_{12}H_{12}N_6Al_6$ and $H_{12}N_{12}AL_{12}$. We evaluated several properties such as adsorption energy, band gap, charge transfer, and dipole moments, COSMO surface analysis. In this research highlighted the active binding sites, and the findings showed that the modified nanosheets significantly improved their binding abilities with drugs under realistic conditions. Additional analyses through ADMET screening and molecular docking suggested that the drug transport efficiency was enhanced by using these doped coronene nanosheets. The binding affinities, indicating the strength of the drug's attachment to key proteins in nucleotide metabolism, were significantly elevated with values of ≤ -7.1 kcal/mol. This was especially pronounced in the nanosheet-drug complexes related to essential proteins like TPMT, TYMP, and TYMS. Among these, the complexes formed between 6-TG and $H_{12}N_{12}Al_{12}$ and $B_{12}N_{12}P_{12}$ stood out for their selective interactions with vital residues. The doping of these nanosheets enhanced binding strength and reduced the likelihood of after effects, resulting in improved overall stability. This research shows that coronene nanosheets altered with $H_{12}N_{12}Al_{12}$ demonstrate significant potential as multi-drug carriers for targeted cancer therapy.

Table of Contents

List of Figures

List of Tables

Abbreviation

Abbreviation	Meaning
DFT	Density Functional Theory
DOS	Density of States
FMO	Frontier Molecular Orbitals
HOMO	Highest Occupied Molecular Orbital
LUMO	Lowest Unoccupied Molecular Orbital
ESP	Electrostatic Potential
NPs	Nanoparticles
GGA	Generalized Gradient Approximation
DNP	Double Numerical with Polarization basis set
DSPP	DFT Semi-core Pseudopotentials
COSMO	Conductor-like Screening Model
QMD	Quantum Molecular Descriptors
MD	Molecular Dynamics
5-FU	5-Fluorouracil
6-TG	6-TGioguanine
6-MP	6-MPrcaptopurine
eV	Electron Volt
TPMT	Thiopurine S-methyltransferase
TYMP	Thymidine Phosphorylase
TYMS	Thymidylate Synthase

Chapter 1

Introduction

1.1 Overview

Cancer has emerged as the leading cause of death globally, with around 20 million new cases and 9.7 million deaths each year. These alarming statistics highlight the urgent necessity to address this widespread disease and its impacts [1]. Cancer arises when the usual regulation of cell division fails, leading to unrestrained cell multiplication and the potential to spread to various regions of the body [2]. The most common methods for treating cancer are chemotherapy, radiation therapy, and surgical procedures [3]. Chemotherapy aims to eliminate the cancerous cells; however, it can also harm healthy cells, resulting in side effects such as fatigue, hair loss, nausea, and vomiting [4], [5], [6].

Fischer et al. utilized dispersion-corrected DFT and AIMD to investigate the adsorption and release of 5-fluorouracil (5-FU) within faujasite-type zeolites, demonstrating that hydrogen bonding with framework protons is crucial for both the adsorption process and the water-initiated release [7]. Rezaei-Sameti et al. explored the relationships between 5-FU and nucleobases by employing QTAIM and RDG methods, demonstrating that the most stable complexes are created between cytosine and guanine [8]. Ibrahim et al. utilized density functional theory (DFT) and molecular dynamics to evaluate the effectiveness of 6-MP and 6-TG as corrosion inhibitors on Al(111) surfaces, highlighting their strong adsorption characteristics and ability to donate electrons [9].

In a research project focused on two-dimensional materials, Mehedi Hasan Opi et al. performed a thorough analysis of graphene, boron nitride (BN), and their doped variations for the delivery of hydroxyurea (HU). They determined that $C_{16}B_{16}N_{16}$ nanostructures demonstrated exceptional adsorption energy and solvation characteristics, attributed to their significant dipole moments and surface polarity [10]. Roy Swarna and colleagues showed that hetero-nanocages like $B_6N_6Al_6N_6$

have enhanced stability and adsorption properties for HU compared to purely nanocages, highlighting the advantages of in-plane doping [11]. Mohammed et al. examined the electronic properties of 6-MP, CP, and GB, revealing their semiconductor characteristics and electron transfer abilities, which suggest their potential for effective integration into nanocarriers [12]. Ahmed B. Bayoumy et al. presented a comprehensive analysis of thiopurine drug delivery techniques, emphasizing challenges concerning solubility and selectivity that can be addressed using nanocarriers [13].

These analyses together highlight the importance of creating drug-targeted and structurally enhanced nanocarriers to enhance cancer treatment outcomes. This research adds to the expanding body of knowledge by performing a comparative study of three anticancer drugs, 5-FU, 6-TG, and 6-MP, using both pristine and heteroatom-doped coronene nanosheets through sophisticated DFT-based simulations.

1.2 Motivation of the Research

Cancer is a deeply personal and heartbreaking issue that affects millions of lives around the world. For many, the journey through treatment can feel overwhelming. While traditional methods like chemotherapy, radiotherapy, and surgery might save lives, they often come with extraordinarily tough challenges. Take medications like 5-Fluorouracil (5-FU), 6-Tioguanine (6-TG), and 6-Mercaptopurine (6-MP) for instance. Although they can help fight cancer, patients frequently struggle with how their bodies absorb these drugs. It can be frustrating when the medications break down too quickly or don't work as intended. On top of that, the side effects can be grueling, making it hard for patients to stick to their treatment plans. These hurdles highlight an urgent need for more innovative and effective ways to deliver cancer treatments methods that are better targeted and designed with fewer side effects in mind. The ultimate goal is to make this incredibly tough journey a bit easier and more effective for those fighting this battle, allowing them to focus on what really matters: their health, their loved ones, and their lives. In recent years, scientists have explored nanotechnology as an encouraging path to address these issues. Nanocarriers minute materials like graphene, boron nitride (BN), and coronene-based structures provide promising advantages. Their large surface area and customizable characteristics can enhance drug solubility and stability while enabling controlled release, making them strong contenders for more focused

cancer therapies. However, there is still much to discover regarding how these nanocarriers interact with cancer medications like 5-FU, 6-TG, and 6-MP, particularly concerning drug absorption and release. Research conducted by teams such as Mehedi Hasan Opi et al. has shown that specific BN structures can improve the stability of drug absorption, while discoveries made by Rezaei-Sameti et al. emphasize the importance of drug-DNA interactions in enhancing drug effectiveness. This investigation intends to optimize the design of these nanocarriers by utilizing advanced simulation techniques such as Density Functional Theory (DFT) and Ab Initio Molecular Dynamics (AIMD). Fischer et al. have been doing some fascinating research that focuses on how materials behave under conditions similar to those found in the human body. This groundbreaking work is opening new doors for targeted cancer treatments, which means that scientists can develop therapies that are much more tailored to the specific needs of patients.

This research aims to deepen our understanding of how anticancer drugs interact with coronene-based nanocarriers. By using DFT simulations, we will look into important factors like how well the drugs attach to the carriers and how they are released. The ultimate goal is to create a more comprehensive approach to designing drug delivery systems. We genuinely believe that by taking this approach, we can improve the way cancer treatments work while also reducing the side effects. Our goal is to offer patients more personalized and effective options in their fight against cancer, making their journey a bit easier.

1.3 Problem Statement

Cancer is a significant health challenge that touches the lives of millions of people around the world every year. Despite the incredible progress we've made in medical science, cancer still stands as one of our most formidable foes. For a long time, treatments like chemotherapy, radiotherapy, and surgery have been the go-to strategies to combat this disease. While these methods can sometimes be effective at targeting and eliminating cancer cells, they also come with some tough side effects.

Consider chemotherapy, for example. It not only targets cancer cells but can also affect healthy ones, resulting in exhausting side effects such as fatigue, hair loss, nausea, and a weakened immune system. While radiotherapy is an important treatment option, it presents its own challenges. Regarding tumor treatment, we have several potent methods available, but they come with

difficulties. For instance, although radiation can be effective against tumors, it may also damage the surrounding healthy tissue. Such damage may lead to painful skin burns and could raise the chances of developing new cancers later on. On the other hand, surgery may be a viable choice, particularly for tumors that haven't significantly metastasized. Nonetheless, it comes with its own risks, such as the potential for infections and other complications during the recovery process.

There remains a lot to learn about the functioning of these advanced materials, particularly regarding their interactions with pharmaceuticals. This study aims to investigate these interactions in more depth by assessing various coronene nanostructures for their capacity to transport specific anti-cancer medications: 5-FU, 6-TG, and 6-MP. By conducting thorough simulations, we will evaluate the efficiency of these nanocarriers in drug uptake, examine the nature of their electronic interactions, and assess their overall effectiveness in treatment delivery. Our ultimate goal is to identify the most effective nanocarrier for each drug while taking into account how their features might reduce side effects and improve treatment effectiveness.

1.4 Research Questions

This study is driven by the following core research questions:

1. How do the three anticancer drugs (5-FU, 6-TG, and 6-MP) adsorb onto different nanocarrier models?
2. What is the relationship between nanocarrier properties, such as adsorption energy, HOMO-LUMO gap, dipole moments, and charge transfer, with the reduction of side effects?
3. Which nanocarrier shows the best performance in drug delivery for 5-FU, 6-TG, and 6-MP?

1.5 Research Objectives

The primary objectives of this research are:

1. The goal is to study the adsorption of three anticancer drugs 5-Fluorouracil (5-FU), 6-Thioguanine (6-TG), and 6-Mercaptopurine (6-MP) onto nanocarriers to understand their molecular interactions.
2. To analyze and reduce side effects associated with conventional chemotherapy drugs by evaluating adsorption energy, HOMO-LUMO band gap, dipole moments, charge transfer, and solvation energy.
3. To identify and optimize the most efficient nanocarrier based on their drug adsorption capacity, electronic properties, in order to improve therapeutic efficacy in anticancer treatments.

1.6 Research Contributions

This study introduces a detailed computational framework aimed at examining coronene-based nanostructures for the purpose of delivering anticancer medications such as 5-Fluorouracil (5-FU), 6-Thioguanine (6-TG), and 6-Mercaptopurine (6-MP). The research utilizes Density Functional Theory (DFT) to investigate the adsorption properties, electronic interactions, and mechanisms of drug release associated with these nanocarriers. The major contributions of this study are as follows:

1. **In-Depth Analysis of Coronene Nanocarriers for Drug Delivery:** The study presents the first comprehensive comparison of unmodified and doped coronene nanostructures concerning the delivery of 5-FU, 6-TG, and 6-MP. By analyzing adsorption energy, electronic characteristics, and solvation behavior, the research identifies the most effective nanocarrier for each medication, offering practical insights for improved drug delivery systems (DDS).
2. **Identification of Key Nanocarrier Properties for Drug Delivery:** By examining the impact of adsorption energy, the HOMO-LUMO gap, dipole moments, and charge transfer on the effectiveness of drugs, this study provides a more comprehensive understanding of how these elements relate to drug delivery success. This crucial knowledge assists in focusing efforts to minimize side effects while improving drug retention and effectiveness.
3. **Insights into the Role of Doping in Nanocarrier Performance:** The research offers important insights into how doping with boron, nitrogen, and phosphorus impacts coronene nanostructures, showing that doping improves the adsorption energy and charge transfer

characteristics of the nanocarriers. This advancement aids in creating drug delivery systems that are more efficient, stable, and biocompatible.

4. **Participation in Solvation Modeling for Biocompatible Drug Delivery:** Through the application of the COSMO solvation model, this research extends solvation modeling techniques for thiopurine drugs. It evaluates the influence of aqueous environments on drug release and solubility, providing biologically relevant data that can be used to optimize DDS in real-world conditions.

1.7 Scope of Research

This research delves into how anticancer drugs, specifically 5-FU, 6-TG, and 6-MP, interact with coronene-based nanocarriers, both in their natural form and when enhanced with elements like boron, nitrogen, and phosphorus. To better understand this interaction, we utilize Density Functional Theory (DFT) to look at how well these drugs can attach to the nanocarriers and how effective they are at delivering the drugs.

Our focus is on comparing different types of coronene nanostructures, including both pure and modified versions. We evaluate important factors such as the energy of drug absorption, the electronic characteristics (like the HOMO-LUMO gap), charge transfer capabilities, and how these structures behave in solutions that mimic biological environments. The goal is to pinpoint the most suitable nanocarrier for each drug based on these metrics.

Furthermore, we're aiming to set up criteria for choosing nanocarriers, linking the strength of drug adsorption and their electronic properties to the potential for fewer side effects and enhanced drug effectiveness. By simulating biological conditions in our solvation model, we hope our findings will be applicable in real-world scenarios. In this research, a dataset focusing on electronic, geometric, and solvation aspects was developed. The goal is to develop improved drug delivery systems that lead to more accurate and efficient cancer treatments.

Key Boundaries:

1. The research depends significantly on computational techniques and has not been confirmed through experimental validation.

2. This study zeroes in on a particular group of nanomaterials, rather than looking at every single drug-nanocarrier pairing out there.
3. What we often imagine as perfect conditions might not really match the way things actually are in nature.

1.8 Outline of the Research

Introduction: This section presents the context, motivation, issue description, research inquiries, goals, contributions, and boundaries of the study.

Literature Review: This section provides an in-depth examination of current research regarding interactions between drugs and nanomaterials, emphasizing DFT and associated quantum chemical methods.

Methodology: This section describes the computational methods, including model setup, basis sets, solvation strategies, and optimization approaches.

Results and Discussion: This part assesses the results of the simulations, incorporating HOMO-LUMO analysis, charge density distributions, density of states (DOS) projected density of states (PDOS), and electrostatic potentials.

Conclusion and Future Work: The results are outlined, the constraints are examined, and potential avenues for future studies are emphasized, including experimental validation and progress related to AI.

Chapter 2

Literature Review

2.1 Introduction

In several biological applications, including drug delivery [14], biosensing [15], and bioimaging [16], nanomaterials have been studied because of their unique characteristics and drastically different functioning from their bulk counterparts. An assortment of topologies that have For these applications, nanotubes (NTs) [17], [18], [19], [20], nanowires [21], nanoparticles [22], nanorods [23], and two-dimensional (2D) sheets [24] have all been proposed as substrates. Advancements in nanotechnology have greatly influenced biomedical research, particularly in creating novel drug delivery systems (DDS). These systems seek to address significant challenges linked to traditional cancer treatments, such as systemic toxicity, limited bioavailability, and non-targeted delivery. A promising research focus is on two-dimensional (2D) nanomaterials, especially coronene-based nanosheets. These materials are attractive due to their large surface area, tunable electronic characteristics, and remarkable capacity to adsorb molecules. Scientists have been using a method known as Density Functional Theory (DFT) to investigate the characteristics and behaviors of nanoscale systems at the quantum level. This method allows them to gain deeper insights into how these tiny structures operate. DFT is well-respected for its accuracy and has facilitated a deeper understanding of how these tiny systems interact with biological materials. By augmenting DFT with approaches such as Time-Dependent DFT (TD-DFT) and Ab Initio Molecular Dynamics (AIMD), scientists can create complex simulations that closely represent these interactions. This advanced modeling is essential for comprehending and designing effective nanocarriers capable of safely delivering anticancer medications. The insights gained from this research are crucial for advancing therapies that minimize risks while improving effectiveness.

2.2 Existing Previous Work

Many investigations have utilized Density Functional Theory (DFT) to investigate the interactions between anticancer medications and various nanocarriers. A significant illustration is the research carried out by Rezaei-Sameti et al., in which they studied the binding interactions of 5-fluorouracil (5-FU) with DNA nucleobases. Their findings revealed that cytosine and guanine showed the most significant non-covalent interactions with 5-FU, mainly through hydrogen bonding. The findings were further reinforced by analyses conducted using QTAIM and ELF techniques [8]. The safety and effectiveness of medications, like the chemotherapy drug 5-FU can be influenced by how well they target specific nucleobases. A study conducted by Mohammed and Hanoon investigated the behavior of drugs like 6-mercaptopurine (6-MP), cyclophosphamide (CP), and gemcitabine (GB) on two-dimensional surfaces using first-principles calculations. Their findings reveal that these compounds demonstrate semiconductor-like characteristics, with significant HOMO-LUMO gaps and electronic properties, indicating they may have considerable electron mobility and reactivity, which could improve their effectiveness in treatment [12]. Ibrahim et al. carried out studies on corrosion inhibition that indicated expired thiopurine medications, such as 6-MP and 6-TG, can establish stable interactions with aluminum surfaces. This stability results from their advantageous adsorption energies and charge transfer processes, suggesting their potential as dual-functional agents [9]. In a recent investigation, Fischer et al. examined the interactions between 5-Fluorouracil (5-FU) and faujasite-type zeolites utilizing advanced methods like DFT-D3 and AIMD. The study highlighted the significance of hydrogen bonds formed with the protons in the zeolite framework. These bonds are necessary not only for securing the drug in position but also for boosting its release when water is present [7]. Additionally, a major investigation by Roy Swarna et al. focused on how hydroxyurea (HU) interacts with various hetero-nanocages, specifically $C_{12}B_6N_6$, $C_{12}Al_6N_6$, and $B_6N_6Al_6N_6$. Through density functional theory (DFT) calculations, they discovered that the $B_6N_6Al_6N_6$ configuration demonstrated the strongest adsorption energy and noteworthy charge transfer qualities, especially at the tetragonal ALN sites [11]. Mehedi Hasan Opi et al. conducted a comprehensive analysis using Density Functional Theory (DFT) to assess the effectiveness of graphene, boron nitride (BN), and their in-plane doped variations in delivering the drug hydroxyurea. They discovered that the $C_{16}B_{16}N_{16}$ doped configuration emerged as the most effective choice. This was due to its advantageous combination of dipole moment, solvation stability, and overall reactivity [10]. Ahmed B. Bayoumy et al.

emphasized several key issues related to conventional thiopurine drug delivery techniques. They suggested that the incorporation of nanocarriers could significantly improve therapeutic outcomes while reducing side effects [7]. In a recent investigation, Roy Swarna et al. explored the effectiveness of certain types of hetero-nanocages, with a focus on $B_6N_6Al_6N_6$, regarding their adsorption capabilities. The findings indicated that these nanocages were particularly resilient and formed robust bonds with the drug hydroxyurea (HU). The researchers discovered that the inclusion of boron and aluminum greatly enhanced the interaction between the medication and its carrier, resulting in improved molecular recognition and overall efficacy. These results highlight the significance of material engineering and electronic design in advancing drug-nanocarrier systems.

2.3 Finding Gaps from Previous Work

The advancements are being made in the field of drug delivery systems (DDS), particularly with the use of nanocarriers. Researchers are employing density functional theory (DFT) simulations to explore the interactions between these drugs and their carriers. However, there are still significant factors in this research that could hinder the successful adoption of these innovations.

Lack of Experimental Validation: Numerous studies, such as those by Rezaei-Sameti et al. showcase promising findings from DFT, yet they frequently lack sufficient experimental backing to support their claims regarding drug absorption onto nanocarriers and the stability of these complexes. It is a common challenge in theoretical research to bridge the ideal conditions of simulations with the complexities of biological environments. Various factors like cytotoxicity, immunogenicity, and pharmacokinetics come into play in this context. For instance, although extensive modeling has been performed on 5-FU binding with DNA nucleobases (Rezaei-Sameti et al.), its actual biological function and efficacy in living organisms have not been comprehensively studied.

Oversimplified Biological Models: Another issue is the inclination to utilize simplified models when simulating drug-nanocarrier interactions. Investigations by Roy Swarna et al. and Mehedi Hasan Opi et al. highlight the potential of hetero-nanocages for drug delivery but often do not

accurately represent genuine biological conditions. Despite the application of the COSMO solvation model, it fails to fully encompass the complexities of biological systems, such as protein binding, cellular uptake, and interactions with the immune system, all of which substantially affect the actual efficacy of DDS.

Narrow Focus in Drug and Nanocarrier Comparison: Research conducted by Mehedi Hasan Opi et al., along with insights from Roy Swarna et al. primarily concentrates on specific drugs such as hydroxyurea and 5-FU. Nonetheless, there is often a lack of comparison between different drugs across various nanomaterials. This narrow focus results in gaps in our understanding, especially considering that the effectiveness of nanocarriers can vary greatly based on the interaction between a drug and its carrier. For illustration, while $C_{16}B_{16}N_{16}$ seems to show potential as a nanocarrier for hydroxyurea, the nature of its interaction with other drugs such as 5-FU, 6-TG, and 6-MP is still unclear. Exploring these interactions may lead to significant discoveries.

Incomplete Exploration of Doping Effects: Research by Rezaei-Sameti et al. and Mehedi Hasan Opi et al. often mention how doping can impact nanocarrier performance; however, the effects of varying doping configurations on the adsorption and release dynamics of anticancer drugs are frequently neglected. While doping with elements like Boron, Nitrogen, and Phosphorus may improve adsorption and charge transfer, their long-term stability and biological implications are not comprehensively understood. Additionally, doping could potentially modify the HOMO-LUMO gap, influencing drug release profiles, but this has not been thoroughly examined across a broader range of anticancer medications.

Insufficient Analysis in Biological Environments: Although there has been substantial examination of the electronic interactions between drugs and nanocarriers, much of this research overlooks the complex biological behaviors that occur once the DDS interacts with living systems. Critical factors such as electronic rearrangements and solubility in aqueous environments have not been sufficiently addressed in most studies. These elements are essential for ensuring that nanocarriers can effectively deliver the appropriate dosage of drugs to their intended targets while preserving stability and biocompatibility.

Requirement for Multi-Parameter Optimization: Lastly, while studies like those by Fischer et al. and Mehedi Hasan Opi et al. focus on factors such as adsorption energy and electronic characteristics, they frequently overlook the chance to consider several performance indicators at once. Important metrics, including dipole moments, solvation energy, and other quantum molecular descriptors, should be analyzed collectively to identify the most efficient nanocarrier for each specific drug. Furthermore, research should incorporate multi-dimensional comparisons that take into account electronic reactivity, solubility, adsorption capacity, and drug release profiles; this would assist in identifying the optimal nanocarrier options across various types of drugs. Significant progress has been achieved in the area of nanocarrier-based drug delivery systems (DDS), particularly through the use of DFT simulations that analyze the interactions of drugs with these nanocarriers. Nonetheless, there remain several crucial gaps in the research that could impede the real-world application of these findings.

2.4 Critical Analysis

The advancements we've achieved in drug delivery systems (DDS), especially with the use of nanocarriers, are remarkable. Researchers have utilized density functional theory (DFT) simulations to explore the interactions between medications and these carriers, resulting in some intriguing findings. However, several hurdles remain that need to be tackled for these advancements to be successfully applied in real-world scenarios.

The insufficient experimental validation: Although research conducted by individuals such as Rezaei et al. and Fischer et al. yields encouraging DFT findings, these studies frequently lack the essential experimental support. This lack of tangible data complicates the acceptance of assertions regarding the absorption efficiency of drugs by nanocarriers or the stability of these complexes. The challenge is compounded by the complexities of biological systems; for instance, even though there’s substantial modeling regarding the binding of 5-FU (a chemotherapy drug) to DNA, we still don't fully understand how well it works in living organisms.

Narrow focus on specific drugs: Investigations led by Mehedi Hasan Opi et al. and others often zoom in on certain medications, like hydroxyurea and 5-FU, neglecting a more comprehensive look at various drugs and nanomaterials. This focused viewpoint might overlook potentially beneficial insights, especially since different drugs can have varying interactions with the same nanocarrier. For instance, even though the $C_{16}B_{16}N_{16}$ nanocarrier seems to be a promising option for hydroxyurea, its interactions with other drugs like 5-FU, 6-TG, and 6-MP need further examination.

Doping configurations in nanocarriers: Research from Mehedi Hasan Opi et al. has certainly addressed how elements like boron and nitrogen can influence these carriers, but how these doping processes affect the release of drugs and their interactions remains largely unexplored. Often, the effects of doping on the electronic properties of structures like coronene are oversimplified. There is also a deficiency of thorough research examining how various dopants, such as boron, nitrogen, and phosphorus, influence drug binding and release when considered together.

Concentrate on multiple factors: Many research studies typically concentrate on specific factors like adsorption energy or charge transfer, neglecting a more holistic perspective. While the observations from Fischer et al. offer valuable insights, they often do not evaluate various performance metrics at the same time. Important factors, including solubility, stability, adsorption efficiency, and drug release profiles, need to be analyzed collectively to develop a more comprehensive understanding. This comprehensive method is crucial for determining the most efficient nanocarriers for delivering drugs.

2.5 Summary

This part provides an in-depth examination of the crucial role that nanomaterials, including graphene, boron nitride, and coronene-derived structures, play in drug delivery systems focused on cancer treatment. These materials are highly valued for their remarkable characteristics, such as a high surface area, tunable electronic properties, and their compatibility with biological systems, rendering them exceptional options for targeted drug delivery applications. Investigators such as Rezaei-Sameti et al. and Mohammed et al. have utilized DFT simulations to examine the

interactions between anticancer drugs and these nanocarriers. Their results indicate improved drug attachment and charge transfer, which offers significant potential for therapeutic use. Nonetheless, there are significant shortcomings in the existing research. A considerable number of studies lack experimental validation and tend to excessively use simplified biological models. While researchers like Roy Swarna et al. and Mehedi Hasan Opi et al. have made valuable contributions to understanding the interactions between individual drugs and nanocarriers, they frequently neglect the intricacies involved in comparing multiple drugs or addressing the complexities of real-world biological conditions. Furthermore, the impact of doping on drug release and the long-term stability of these systems has not been adequately investigated.

In summary, although the prospects of nanocarriers for cancer therapy are promising, it is crucial to seek further empirical validation and thorough assessments of their efficacy in order to completely understand their role in fighting cancer.

Chapter 3

Methodology

3.1 Geometry Optimization and Convergence Criteria

The geometry optimization of all molecular systems, including both pristine and doped coronene nanosheets with anticancer drugs, was performed using Density Functional Theory (DFT) implemented in Materials Studio. The calculations were executed with the Perdew–Burke–Ernzerhof (PBE) functional, known for its reliability in forecasting structural and electronic characteristics. For the optimization procedure, the double numerical plus polarization (DNP) basis set was employed, offering exceptional computational accuracy, especially for examining transition states and excited states. Additionally, Density Functional Theory semi-core pseudopotentials (DSPP) were used to effectively consider the core electrons.

The geometry optimization process converged when the following criteria were met:

1. Maximum displacement: 0.005 Å (Angstrom)
2. Maximum force: 0.004 Ha Å−1 (Hartree per Angstrom)
3. Energy convergence tolerance: 2 × 10−5 Ha (Hartree)
4. SCF convergence: 1 × 10−5 eV (electron volts)
5. Smearing point: 0.005 Ha
6. Global cutoff radius in real space: 5 Å (Angstrom)

These standards guarantee that the optimized structures illustrate stable arrangements, where atomic forces are minimized, and the energies are refined to an accurate value.

3.2 Adsorption Energy Calculation

The adsorption energy (E_{ad}) indicates how strongly a drug molecule interacts with a nanocarrier. It is defined as the difference in energy between the created complex and the separate entities that participate. The E_{ad} [25] for every drug-nanosheet complex is determined using the formula below:

$$E_{ad} = E_{complex} - E_{drug} - E_{nanosheet} \quad (1)$$

$E_{complex}$ represents the total energy of the drug-nanosheet complex, while E_{drug} and $E_{nanosheet}$ refer to the energies of the drug and nanosheet in isolation prior to adsorption. This research analyzed calculations in both gas-phase and aqueous-phase, employing the COSMO solvation model to mimic realistic drug delivery scenarios. The adsorption energy (E_{ad}) indicates the strength of the interaction between the drug molecules (5-FU, 6-TG, and 6-MP) and coronene nanosheets; more negative E_{ad} values imply a stronger adsorption and enhanced binding affinity.

In addition to adsorption energy, the study also calculated the following properties:

Charge Transfer (Q): The overall quantity of electron transfer between the nanocarrier and the drug. A positive charge transfer signifies that electrons are being donated to the drug, whereas a negative charge transfer indicates that electrons are being donated by the nanocarrier.

Interaction Distance (d): The least distance separating the drug molecule from the nanocarrier. Reduced distances suggest more robust interactions, improving binding and drug retention.

Air Media: The energy of adsorption is evaluated in a vacuum, mimicking non-aqueous conditions. This method reflects optimal circumstances where the lack of a solvent permits interactions to be determined only by electrostatic and van der Waals forces.

Aqueous Media: The COSMO solvation model is utilized to model the impact of solvents, like water, on the interactions between drugs and nanocarriers. In water-rich environments, polarization significantly affects both the energy of adsorption and electronic properties. Evaluating adsorption energy provides important insights into the stability and effectiveness of drug-nanocarrier systems. Analyzing charge transfer and the distances between interactions aids in assessing the importance and strength of these interactions in drug delivery.

3.3 Frontier Molecular Orbital (FMO) Analysis

Frontier Molecular Orbitals (FMOs), particularly the Highest Occupied Molecular Orbital (HOMO) and the Lowest Unoccupied Molecular Orbital (LUMO), play a critical role in comprehending the reactivity of a substance and its interactions with drug compounds. The energy levels of these orbitals are vital for predicting electronic interactions and reactivity. The HOMO, which represents the highest energy level filled with electrons, offers valuable information about the electron-donating capability of the nanocarrier and its potential to engage with electron-accepting species such as drugs. In contrast, the LUMO signifies the lowest energy level that remains unoccupied and can accept electrons. The energy of the LUMO illustrates the material's capacity to accept electrons, which is vital for promoting electron transfer during the interactions between drugs and nanocarriers. Furthermore, the HOMO-LUMO gap (E_g) refers to the difference in energy between the HOMO and LUMO levels.

$$E_g = E_L - E_H \quad (2)$$

A smaller HOMO-LUMO gap indicates increased reactivity, raising the likelihood that the nanocarrier will interact with drug molecules. This characteristic is particularly crucial for the release of drugs and their targeted delivery, since a smaller gap improves the electrophilic attributes of the nanocarrier, facilitating either the donation or acceptance of electrons with the drug. Additionally, the dipole moment (D.M.) is evaluated to ascertain the polarity of the drug-nanocarrier complex. A greater dipole moment signifies a stronger interaction with polar drug molecules, suggesting enhanced drug loading and targeted delivery potential, particularly within biological systems.

In the frontier molecular orbital (FMO) analysis, the HOMO-LUMO gap, dipole moment, and electronic characteristics are calculated for both air and aqueous environments. This evaluation is essential for understanding how solvation influences the drug-nanocarrier interaction in practical situations.

3.4 DOS Spectra

Comprehending the Density of States (DOS) is essential for clarifying the arrangement of electronic states within a carrier complex at different energy levels. The engagement of drug molecules with this carrier brings about new electronic states that often overlap with existing ones,

thus altering the overall energy landscape. A notable consequence of such interactions is the enhancement of the electronic states' density in proximity to the Fermi level the energy level at which electrons are predominantly situated. An increased density in this region indicates a diminishment of the energy gap between filled and unfilled electronic states within the system. To achieve a deeper comprehension, researchers may examine the Projected Density of States (PDOS), which assists in identifying the contributions of specific atoms or orbitals to the electronic structure. Analyzing PDOS spectra helps recognize the atomic orbitals that engage directly with the drug molecules when they bind. When drug molecules bind to the carrier complex, the energy levels of particular atomic orbitals can change due to variations in the local environment. These alterations can bring energy levels closer to the Fermi level, thereby further narrowing the energy gap between occupied and unoccupied states. Furthermore, the interaction with drug molecules can alter the hybridization of atomic orbitals, which results in the creation of new electronic states within the energy gap. These hybrid states also play a role in decreasing the energy gap, as demonstrated by the density of states (DOS) spectra. The combination of DOS and projected density of states (PDOS) evaluations offers crucial insights into the electronic configuration of carrier complexes used in drug delivery, illustrating how drug interactions can influence the energy landscape. To sum up, the noted reduction in the energy gap, as depicted in the spectra, underscores the complex interplay between carrier materials and drug molecules, which can substantially affect the efficacy and kinetics of drug delivery. Additionally, the conductivity of these nanosheets is significantly enhanced due to the decreased energy gap, demonstrating a strong connection between these electronic modifications and their practical implications in drug delivery systems [26]

$$\sigma \propto e^{-Eg/2KT} \quad (3)$$

where, K is Boltzmann's constant = 1.380×10^{-23} m^2 kg^{-2} k^{-1}.

This analysis helps to determine how drug adsorption impacts the nanocarrier's conductivity, reactivity, and overall stability.

3.5 Electronic Structures and Charge Transfer Analysis

In this section, we explore the electronic properties of drug-nanocarrier complexes by utilizing electron density (ED) maps and electrostatic potential (ESP) maps to understand the charge distribution and the strength of interactions between the drug and the nanocarrier.

ED Maps: Electron Density is the electron arrangement inside the system. It shows how electrons are exchanged between the drug and the nanocarrier during the adsorption phase.

ESP Maps: The electrostatic potential of the complex indicates, emphasizing the alterations in charge distribution that occur as a result of the interaction between the drug and the nanocarrier.

Mulliken Analysis: Measures the distribution of electron density across specific atoms in both the drug and the nanocarrier, illustrating whether the drug acts as an electron donor or acceptor.

Hirshfeld Analysis: Offers a broader assessment of the overlap in electron density and the transfer of charge between the two interacting entities.

These evaluations assist in quantifying electrostatic interactions, which directly affect the strength of adsorption and the dynamics of drug release.

3.6 Dipole Moment Analysis

The dipole moment (D.M.) acts as a key parameter for understanding the polarity of the drug-nanocarrier system. A higher dipole moment signifies that the system has a greater ability to interact with polar drugs and establish stable complexes between the drug and the nanocarrier. The dipole moment is assessed after the adsorption procedure, and examining dipole moments in both air and water environments offers valuable insights into how solvent conditions affect drug-nanocarrier interactions. An elevated dipole moment after adsorption indicates a more robust polar interaction and improved retention of the drug in aqueous environments, which is essential for enhancing drug bioavailability.

3.7 Quantum Molecular Descriptors

Quantum molecular descriptors help assess the reactivity and stability of the drug-nanocarrier system by providing deeper insights into the electronic structure and interaction dynamics. The quantum molecular descriptors were also calculated toward 5-FU, 6-TG, 6-MP by the following equations:

Hardness(η) [27] : Measures the resistance to electron deformation.

$$\text{Hardness, } \eta = (E_{LUMO} - E_{HUMO}) / 2 \quad (4)$$

Global softness(s) [28] : Indicates the susceptibility to electron donation, the inverse of hardness.

$$s = 1/2\eta \quad (5)$$

Chemical potential(μ) [29] : The tendency of the system to donate or accept electrons.

$$\text{Chemical potential, } \mu = - (E_{LUMO}+E_{HOMO}) / 2 \quad (6)$$

Electrophilicity index (ω) [30] : Indicates the system's capability to take in electrons.

$$\text{Electrophilicity index, } \omega = \mu^2 / 2 \quad (7)$$

Nucleophilicity index(υ) [31] : Assesses the system's capacity to provide electrons.

$$\text{Nucleophilicity index, } \upsilon = 1 / \omega \quad (8)$$

These characteristics aid in evaluating the responsiveness of the drug-nanocarrier system and forecasting the way the drug will engage with the nanocarrier throughout the drug delivery process.

3.8 Solvation Energy

The solvation energy (E_{solv}) represents the energy difference between the system in water and the system in air:

$$E_{solv} = E_{water} - E_{air} \quad (9)$$

The COSMO solvation model is used to simulate the solvent effect and understand how the drug-nanocarrier complex behaves in biological environments (i.e., water). Figure 18, 19, and 20 illustrate the COSMO surfaces of the drug-nanosheet complexes, showing how solvation impacts adsorption energy and electronic properties.

This evaluation aids in understanding how solvent interactions influence the stability and effectiveness of the drug-nanocarrier complex in practical conditions.

3.9 Summary

The approach based on DFT employed in this study combines geometry optimization, calculations of adsorption energy, evaluations of electronic properties, investigations of charge transfer, and the impact of solvation to thoroughly examine the interactions between drugs and nanocarriers. The results offer vital insights into how doping can enhance the effectiveness of nanocarriers and the role solvation plays in drug delivery within biological settings. This method lays a strong groundwork for the creation of optimized drug delivery systems, especially for cancer treatments.

Chapter 4

Results and Discussion

This section outlines the results of a computational investigation into the interactions between both pure and doped coronene nanosheets and three anticancer drugs: 5-Fluorouracil (5-FU), 6-Thioguanine (6-TG), and 6-Mercaptopurine (6-MP), utilizing Density Functional Theory (DFT). The study focuses on important factors like adsorption energy, electronic characteristics, charge transfer, dipole moments, solvation effects, and the stability of the complexes formed between the drugs and nanosheets. These findings shed light on the role of doping in affecting the interactions between drug molecules and nanosheets, underscoring considerable implications for advancing more efficient drug delivery systems.

4.1 Optimized Geometric Structures

In this research, pristine coronene ($C_{24}H_{12}$), a polycyclic aromatic hydrocarbon (PAH) consisting of 24 carbon atoms and 12 interconnected benzene rings, was selected as the main model to study its interactions with the anticancer drugs 5-Fluorouracil (5-FU), 6-Thioguanine (6-TG), and 6-Mercaptopurine (6-MP). Coronene is regarded as a suitable candidate for drug adsorption uses, particularly in the development of nanocarriers, due to its extensive surface area, planar configuration, and conjugated π-system. To improve the interactions between the nanosheet and the drug, the initial coronene nanosheet was altered through heteroatom doping, introducing boron (B), nitrogen (N), and phosphorus (P) atoms at different doping levels. The doping configurations examined in this study consisted of 16.67% Boron (B) doping, 16.67% Nitrogen (N) doping, 11.11% Phosphorus (P) doping, and a combined doping of Boron (B), Nitrogen (N), and Phosphorus (P) at 33.33% each. These combinations of doping were selected to represent different scenarios that might enhance electronic properties, adsorption abilities, and interactions between the drugs and nanosheets. The five nanosheet models investigated in this study include:

1. Pristine Coronene ($C_{24}H_{12}$)
2. Boron and Nitrogen doped coronene ($C_{12}H_{12}B_6N_6$)

3. Boron and Nitrogen doped coronene with equal proportions ($H_{12}B_{12}N_{12}$)
4. Boron, Nitrogen, and Phosphorus doped coronene ($C_{12}H_8B_6N_6P_4$)
5. Boron, Nitrogen, and Phosphorus doped coronene ($B_{12}N_{12}P_{12}$)
6. Nitrogen and Aluminum doped coronene ($C_{12}H_{12}N_6Al_6$)
7. Nitrogen and Aluminum doped coronene ($H_{12}N_{12}AL_{12}$)

For every configuration, geometry optimization was performed using DFT calculations to minimize the total energy of each structure. The optimization process verified that all geometries were stable, as there were no imaginary frequencies, indicating that they represented minimum energy configurations. Pristine coronene was optimized to retain its planar, conjugated structure, preserving the integrity of the benzene rings. In the case of the doped coronene nanosheets, doping atoms were strategically positioned to ensure an even distribution across the nanosheet, with the goal of enhancing surface reactivity and examining their effects on electronic properties such as charge distribution and polarizability. Following the optimization process, the drug-nanosheet complexes were assessed for important structural characteristics such as bond lengths, distortions in bond angles, and the surface accessibility for drug adsorption. Notable alterations were observed in bond elongation near the doping sites, indicating a heightened interaction potential due to the electrostatic and polar influences introduced by the doping elements. These optimized configurations offer important insights into the stability, reactivity, and drug adsorption capability of the doped coronene nanosheets, laying the groundwork for further exploration of the adsorption energies, the interactions between the drugs and the nanosheets, and the potential for drug delivery of each configuration.

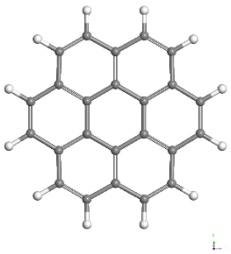

(a)$C_{24}H_{12}$

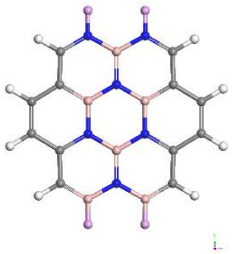

(b)$H_{12}B_{12}N_{12}$

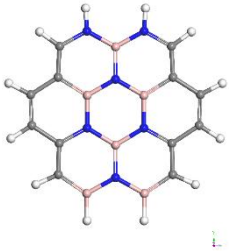

(c)$C_{12}H_{12}B_6N_6$

(d)$B_{12}N_{12}P_{12}$

(e)$C_{12}H_8B_6N_6P_4$

(f)$H_{12}N_{12}AL_{12}$

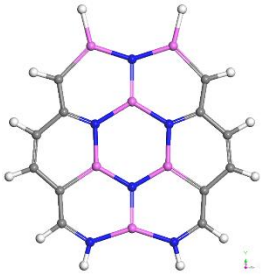

(**g**) $C_{12}H_{12}N_6Al_6$

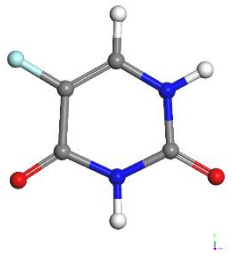

(h)5-FU

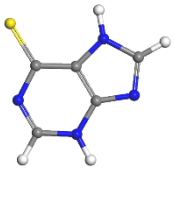

(**i**) 6-Mercaptopurine

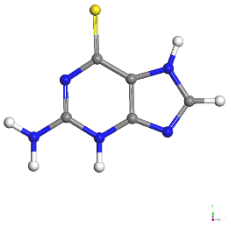

(j) 6-Thioguanine

Figure 1 : Optimized Geometric structures

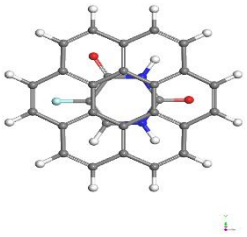

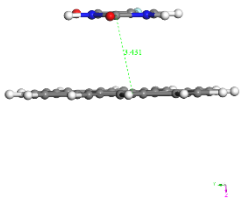

(a) 5-FU/$C_{24}H_{12}$

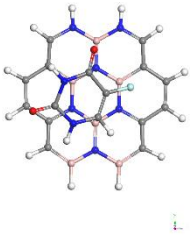

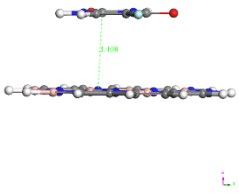

(b)5-FU/$C_{12}H_{12}B_6N_6$

(c) 5-FU/$H_{12}B_{12}N_{12}$

d) 5-FU/$C_{12}H_8B_6N_6P_4$

(e)5-FU/$B_{12}N_{12}P_{12}$

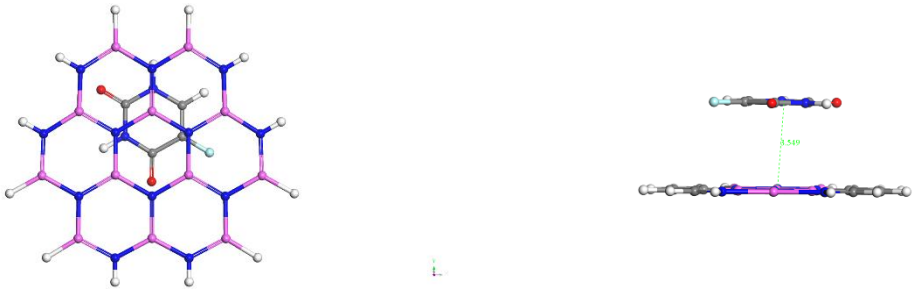

(f) 5-FU/ $H_{12}N_{12}AL_{12}$

(g) 5-FU/$C_{12}H_{12}N_6AL_6$

Figure 2 : Top and side views of the optimized complexes: (a) 5-FU/$C_{24}H_{12}$ (b) 5-FU/$C_{12}H_{12}B_6N_6$ (c) 5-FU/$H_{12}B_{12}N_{12}$ (d) 5-FU/$C_{12}H_8B_6N_6P_4$ and (e) 5-FU/$B_{12}N_{12}P_{12}$ (f) 5-FU/ $H_{12}N_{12}AL_{12}$ (g) 5-FU/$C_{12}H_{12}N_6AL_6$.

(a) 6-TG/$C_{24}H_{12}$

(b) 6-TG/$C_{12}H_{12}B_6N_6$

(c) 6-TG/ $H_{12}B_{12}N_{12}$

(d) 6-TG/ $C_{12}H_8B_6N_6P_4$

(e) 6-TG/$B_{12}N_{12}$ P_{12}

(f) 6-TG/$H_{12}N_{12}AL_{12}$

(g) 6-TG/$C_{12}H_{12}N_6AL_6$

Figure 3 : Top and side views of the optimized complexes: (a) 6-TG/$C_{24}H_{12}$ (b) 6-TG/$C_{12}H_{12}B_6N_6$ (c) 6-TG/$H_{12}B_{12}N_{12}$ (d) 6-TG/$C_{12}H_8B_6N_6P_4$ and (e) 6-TG/$B_{12}N_{12}P_{12}$ (f) 6-TG / $H_{12}N_{12}AL_{12}$ (g) 6-TG/$C_{12}H_{12}N_6AL_6$.

(a) 6-MP/$C_{24}H_{12}$

(b) 6-MP/$C_{12}H_{12}B_6N_6$

(c) 6-MP/$H_{12}B_{12}N_{12}$

(d) 6-MP/$C_{12}H_8B_6N_6P_4$

(e) 6-MP/$B_{12}N_{12}$ P_{12}

(f) 6-MP/$H_{12}N_{12}AL_{12}$

(g) 6-MP/$C_{12}H_{12}N_6AL_6$.

Figure 4 : Top and side views of the optimized complexes: (a) 6-MP/$C_{24}H_{12}$ (b) 6-MP/$C_{12}H_{12}B_6N_6$ (c) 6-MP/$H_{12}B_{12}N_{12}$ (d) 6-MP/$C_{12}H_8B_6N_6P_4$ and (e) 6-MP/$B_{12}N_{12}P_{12}$ (f) 6-MP/$H_{12}N_{12}AL_{12}$ (g) 6-MP/$C_{12}H_{12}N_6AL_6$.

4.2 Adsorption Analysis

The interaction between anticancer drugs (5-FU, 6-TG, and 6-MP) and different pristine and doped coronene nanosheets was assessed for adsorption energy (E_{ad}), charge transfer (Q), and minimum interaction distance (d) in both air and aqueous environments. The findings from these evaluations are shown in the subsequent tables, which provide details on the adsorption energy (in eV), charge transfer (in e), and minimum interaction distance (in Å):

5-FU Adsorption

	Air media			**Water media**		
Structures	**E_{ad}(eV)**	**Q(e)**	**d(Å)**	**E_{ad}(eV)**	**Q(e)**	**d(Å)**
5-FU/$H_{12}B_{12}N_{12}$	-0.2832	−0.197	3.475	-0.1976	−0.085	3.463
5-FU/$C_{12}H_{12}B_6N_6$	-0.2832	−0.016	3.408	-0.1599	−0.045	3.446
5-FU/$B_{12}N_{12}P_{12}$	-0.5020	−0.102	3.406	-0.2591	−0.043	3.435
5-FU/$C_{12}H_8B_6N_6P_4$	-0.3384	−0.029	3.397	-0.1935	−0.037	3.397
5-FU/$H_{12}N_{12}AL_{12}$	-0.2792	−0.134	3.540	-0.1323	−0.119	3.537
5-FU/$C_{12}H_{12}N_6AL_6$	-0.1839	−0.045	3.549	-0.0678	−0.033	3.549

Table 1 : Calculated adsorption energy (E_{ad}) in (eV), charge transfer (Q) in (e), and minimum interaction distance (d) in (Å).

Adsorption Energy:

In air, the interaction between 5-FU and the nanocarriers was most pronounced with $B_{12}N_{12}P_{12}$, which demonstrated an adsorption energy of –0.5020 eV, indicating a strong binding affinity due to the presence of boron nitride and phosphorus atoms. Conversely, $C_{12}H_{12}B_6N_6$ and $H_{12}B_{12}N_{12}$ showed lower adsorption energies of –0.2832 eV, while $C_{12}H_8B_6N_6P_4$ and $H_{12}N_{12}Al_{12}$ exhibited moderate binding energies of –0.3384 eV and –0.2792 eV, respectively. The weakest interaction was observed on $C_{12}H_{12}N_6Al_6$, at –0.1839 eV.

In water, the trend continued, with $B_{12}N_{12}P_{12}$ once more revealing the highest adsorption energy of –0.2591 eV, underscoring its strong potential as a drug delivery carrier in aqueous environments. Other doped structures, such as $C_{12}H_8B_6N_6P_4$ and $H_{12}B_{12}N_{12}$, demonstrated adsorption energies of –0.1935 eV and –0.1976 eV, respectively, while $C_{12}H_{12}B_{12}$.

Charge Transfer:

During the air phase, the highest charge transfer was observed with $H_{12}B_{12}N_{12}$ (–0.197 e), indicating a considerable exchange of electrons between the drug and the nanocarrier, which may impact stability. $B_{12}N_{12}P_{12}$ exhibited a notable charge transfer as well (–0.102 e), whereas compounds like $C_{12}H_{12}B_6N_6$ and $C_{12}H_8B_6N_6P_4$ demonstrated relatively minimal values (–0.016 e and –0.029 e, respectively). $C_{12}H_{12}N_6Al_6$ showed the lowest charge transfer at –0.045 e.

In the context of water, there was a slight shift in the trend. $H_{12}N_{12}Al_{12}$ exhibited the greatest charge transfer (–0.119 e), closely succeeded by $H_{12}B_{12}N_{12}$ with (–0.085 e). In contrast, $B_{12}N_{12}P_{12}$, $C_{12}H_8B_6N_6P_4$, and $C_{12}H_{12}N_6Al_6$ revealed comparable values between –0.043 e and –0.037 e, indicating moderate electronic interactions with 5-FU in water.

Interaction Distance:

The compound with the shortest interaction distance in both air and water was $C_{12}H_8B_6N_6P_4$, with a measurement of 3.397 Å. This small distance implies a stronger attraction of 5-FU to this compound. In a similar vein, $B_{12}N_{12}P_{12}$ exhibited interaction distances of 3.406 Å in air and 3.435 Å in water, whereas $C_{12}H_{12}B_6N_6$ reported distances of 3.408 Å in air and 3.446 Å in water,

emphasizing favorable interactions and strong compatibility with the drug molecule. On the other hand, compounds such as $H_{12}N_{12}Al_{12}$ and $C_{12}H_{12}N_6Al_6$ showed slightly greater distances (approximately 3.54 Å), which could suggest a weaker interaction in comparison to the phosphorus-doped compounds.

6-TG Adsorption

	Air media			Water media		
Structures	**E_{ad}(eV)**	**Q(e)**	**d(Å)**	**E_{ad}(eV)**	**Q(e)**	**d(Å)**
6-TG/$H_{12}B_{12}N_{12}$	1.5926	0.076	3.392	1.7533	0.119	3.392
6-TG/$C_{12}H_{12}B_6N_6$	1.6555	0.112	3.420	1.8135	0.167	3.312
6-TG/$B_{12}N_{12}P_{12}$	1.1786	0.047	3.296	1.4809	0.202	3.296
6-TG/$C_{12}H_8B_6N_6P_4$	1.5173	0.11	3.389	1.7071	0.186	3.408
6-TG/$H_{12}N_{12}AL_{12}$	1.4628	0.001	3.554	1.6785	0.076	3.546
6-TG/$C_{12}H_{12}N_6AL_6$	1.5403	0.115	3.476	1.7280	0.21	3.383

Table 2 : Calculated adsorption energy (E_{ad}) in (eV), charge transfer (Q) in (e), and minimum interaction distance (d) in (Å).

Adsorption Energy:

In the presence of air, $C_{12}H_{12}B_6N_6$ demonstrated the most significant adsorption of 6-TG, reaching the highest adsorption energy of 1.6555 eV, indicating a strong bond between the drug and the nanocarrier. $C_{12}H_{12}N_6Al_6$ (1.5403 eV) and $C_{12}H_8B_6N_6P_4$ (1.5173 eV) also showed considerable binding. In contrast, $B_{12}N_{12}P_{12}$ had the lowest adsorption energy (1.1786 eV), suggesting a comparatively weaker interaction in air. In aqueous environments, all systems demonstrated higher adsorption energies, reflecting enhanced solvation effects. The $C_{12}H_{12}B_6N_6$ system achieved the greatest value at 1.8135 eV, with $C_{12}H_{12}N_6Al_6$ closely following at 1.7280 eV and $C_{12}H_8B_6N_6P_4$ at 1.7071 eV. Although $B_{12}N_{12}P_{12}$ exhibited the lowest interaction in water, its adsorption energy still increased to 1.4809 eV.

Charge Transfer:

In air, the most significant charge transfer was seen with $C_{12}H_{12}N_6Al_6$ (0.115 e) and $C_{12}H_{12}B_6N_6$ (0.112 e), indicating strong electronic interactions and possible charge redistribution between 6-

TG and the carriers. $C_{12}H_8B_6N_6P_4$ and $H_{12}B_{12}N_{12}$ followed closely behind. $H_{12}N_{12}Al_{12}$ showed the lowest charge transfer (0.001 e), suggesting minimal electronic exchange. In water, the $C_{12}H_{12}N_6Al_6$ system once again demonstrated the greatest charge transfer (0.210 e), showing increased interaction in aqueous conditions. $B_{12}N_{12}P_{12}$ (0.202 e) and $C_{12}H_{12}B_6N_6$ (0.167 e) also exhibited considerable charge exchange. This pattern emphasizes how solvation can affect charge redistribution and enhance interactions.

Interaction Distance:

The shortest interaction distances were recorded for $B_{12}N_{12}P_{12}$ (3.296 Å in both conditions), indicating close proximity and the potential for effective drug loading, even though its adsorption energy is lower. $C_{12}H_{12}B_6N_6$ (3.312 Å in water) and $C_{12}H_{12}N_6Al_6$ (3.383 Å in water) also showed relatively strong binding. Conversely, $H_{12}N_{12}Al_{12}$ displayed the greatest distances (3.554 Å in air and 3.546 Å in water), which aligns with its low charge transfer and moderate adsorption energy, signifying weaker binding.

6-MP Adsorption

	Air media			**Water media**		
Structures	**E_{ad}(eV)**	**Q(e)**	**d(Å)**	**E_{ad}(eV)**	**Q(e)**	**d(Å)**
6-MP/$H_{12}B_{12}N_{12}$	4.2755	0.008	3.399	4.4243	-0.017	3.421
6-MP/$C_{12}H_{12}B_6N_6$	1.6118	0.062	3.431	1.7481	0.057	3.423
6-MP/$B_{12}N_{12}P_{12}$	1.2510	−0.022	3.332	1.5114	0.069	3.332
6-MP/$C_{12}H_8B_6N_6P_4$	1.5348	0.045	3.388	1.6859	0.065	3.338
6-MP/$H_{12}N_{12}AL_{12}$	1.4641	−0.068	3.551	1.6286	–0.038	3.551
6-MP/$C_{12}H_{12}N_6AL_6$	1.5660	0.046	3.349	1.7066	0.072	3.349

Table 3 : Calculated adsorption energy (E_{ad}) in (eV), charge transfer (Q) in (e), and minimum interaction distance (d) in (Å).

Adsorption Energy:

In air, the highest adsorption energy was seen with $H_{12}B_{12}N_{12}$ at 4.2755 eV, indicating a very strong interaction between 6-MP and this nanocarrier. However, this extremely high value may suggest non-typical adsorption behavior (possibly over binding or chemisorption). Among the doped structures, $C_{12}H_{12}B_6N_6$ (1.6118 eV), $C_{12}H_{12}N_6Al_6$ (1.5660 eV), and $C_{12}H_8B_6N_6P_4$ (1.5348 eV)

showed strong but more physically realistic interactions. $B_{12}N_{12}P_{12}$ had the lowest adsorption energy (1.2510 eV), reflecting weaker interaction in air. In water, the overall adsorption energies increased across all nanocarriers. $H_{12}B_{12}N_{12}$ again showed the highest adsorption energy (4.4243 eV), followed by $C_{12}H_{12}B_6N_6$ (1.7481 eV) and $C_{12}H_{12}N_6Al_6$ (1.7066 eV), reinforcing their strong binding capabilities with 6-MP. The $B_{12}N_{12}P_{12}$ system, despite being structurally compact, continued to display the lowest energy (1.5114 eV) among all.

Charge Transfer:

In air, most nanocarriers exhibited modest positive charge transfer, with $C_{12}H_{12}B_6N_6$ (0.062 e) and $C_{12}H_{12}N_6Al_6$ (0.046 e) showing the highest electron donation from the nanocarrier to the 6-MP drug. Interestingly, $H_{12}N_{12}Al_{12}$ had a negative charge transfer (–0.068 e), suggesting some electron withdrawal by the nanocarrier. $H_{12}B_{12}N_{12}$ exhibited minimal charge interaction (0.008 e), despite its strong adsorption energy. In water, the trend persisted with enhanced charge transfers. $C_{12}H_{12}N_6Al_6$ showed the highest charge transfer (0.072 e), closely followed by $B_{12}N_{12}P_{12}$ (0.069 e) and $C_{12}H_8B_6N_6P_4$ (0.065 e). Notably, $H_{12}B_{12}N_{12}$ displayed negative charge transfer (–0.017 e) in water, contrasting with its positive value in air, possibly due to solvent-induced charge polarization.

Interaction Distance:

The shortest interaction distances were consistently observed with $B_{12}N_{12}P_{12}$ and $C_{12}H_{12}N_6Al_6$, both at 3.332–3.349 Å, suggesting tight binding and efficient surface contact with 6-MP. $C_{12}H_8B_6N_6P_4$ also performed well with a distance of 3.338 Å in water. In contrast, $H_{12}N_{12}Al_{12}$ had the largest interaction distances (3.551 Å in both media), indicating relatively looser binding, which may reduce drug-carrier stability.

Analysis

The analysis of 5-fluorouracil (5-FU), 6-TGioguanine (6-TG), and 6-MPrcaptopurine (6-MP) on various nanocarriers reveals distinct adsorption characteristics, with each drug showing unique interactions based on adsorption energy (Ead), charge transfer (Q), and interaction distance (d). 5-FU demonstrated the strongest interaction with $B_{12}N_{12}P_{12}$, both in air (–0.5020 eV) and water (–0.2591 eV), suggesting that doping significantly enhances the drug-nanocarrier interaction for efficient binding and stability in drug delivery systems. 6-TG exhibited the strongest adsorption with $C_{12}H_{12}B_6N_6$, showing the highest adsorption energy (–1.6555 eV in air, –1.8135 eV in water), making it an ideal candidate for nanocarrier-based delivery, especially in aqueous environments, where stronger binding is beneficial. 6-MP showed a remarkably strong binding to $H_{12}B_{12}N_{12}$ (with adsorption energies of 4.2755 eV in air and 4.4243 eV in water), but this could suggest potential over binding, which may hinder controlled release. $C_{12}H_{12}B_6N_6$ and $C_{12}H_{12}N_6Al_6$ also performed well but with more balanced interactions.

In summary, 5-FU is best suited for $B_{12}N_{12}P_{12}$-based carriers, 6-TG for $C_{12}H_{12}B_6N_6$, and 6-MP for $H_{12}B_{12}N_{12}$, with each drug exhibiting optimized interactions for efficient drug delivery depending on the nanocarrier composition.

4.3 Frontier Molecular Orbital (FMO) Analysis

To gain a deeper understanding of the interaction between nanocarriers and drugs, we investigated their electronic characteristics by examining the Frontier Molecular Orbitals (FMOs). In particular, we concentrated on the Highest Occupied Molecular Orbital (HOMO) and the Lowest Unoccupied Molecular Orbital (LUMO) of each optimized complex. Analyzing these orbitals provides us with important insights into the distribution of charges and the movement of electrons within the systems.

The HOMO indicates potential locations for electron donation, while the LUMO reveals where electrons may be accepted. This spatial configuration is essential for anticipating the behavior of these nanocarriers when they come into contact with anticancer medications such as 5-Fluorouracil (5-FU), 6-Thioguanine (6-TG), and 6-Mercaptopurine (6-MP). In our visualizations, blue lobes denote the HOMO regions with high electron density, suggesting potential sites for electron donation, whereas yellow lobes illustrate the LUMO areas that are capable of accepting electrons. These diagrams demonstrate how the electronic cloud's distribution changes upon the formation of complexes with drug carriers. Furthermore, we investigated the impact of doping the nanosheets with elements like Boron (B), Nitrogen (N), or Phosphorus (P) on these orbitals. A more localized or overlapping distribution of the HOMO and LUMO indicates stronger interactions, which could enhance drug binding, facilitate charge transfer, and improve release in biological settings.

HOMO **LOMO**

(a) 5-FU/$C_{24}H_{12}$

(b) 5-FU/$C_{12}B_6N_6H_{12}$

(c) 5-FU/$B_{12}N_{12}H_{12}$

(d) 5-FU/$B_{12}N_{12}H_8P_4$

(e) 5-FU/$B_{12}N_{12}P_{12}$

(f) 5-FU/$H_{12}N_{12}AL_{12}$

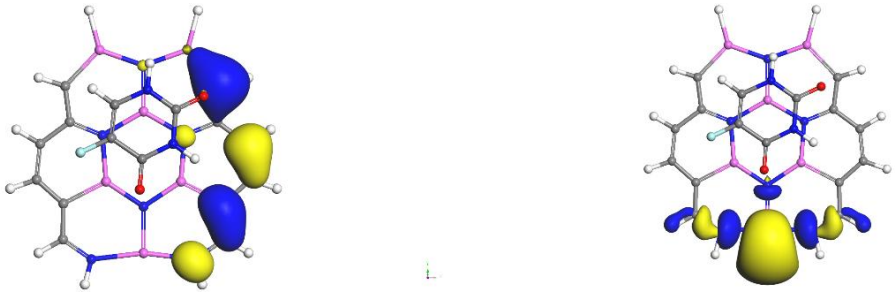

(g) 5-FU/$C_{12}H_{12}N_6AL_6$

Fig. 3 HOMO and LUMO maps of the complexes.

Figure 5 : HOMO and LUMO maps of the complexes (5-FU + Coronene) (a) 5-FU/$C_{24}H_{122}$, (b) 5-FU/$C_{12}B_6N_6H_{126}$ (c) 5-FU/ $B_{12}N_{12}H_{12}$, (d) 5-FU/$B_{12}N_{12}H_8P_4$ and (e) 5-FU/$B_{12}N_{12}P_{12}$ (f) 5-FU / $H_{12}N_{12}AL_{12}$ (g) 5-FU/$C_{12}H_{12}N_6AL_6$.

HOMO **LOMO**

(a) 6-TG/$C_{24}H_{12}$

(b)6-TG/$C_{12}H_{12}B_6N_6$

(c) 6-TG/$H_{12}B_{12}N_{12}$

(d)6-TG/$C_{12}H_8B_6N_6P_4$

(e)6-TG/$B_{12}N_{12}P_{12}$

(f) 6-TG/$H_{12}N_{12}AL_{12}$

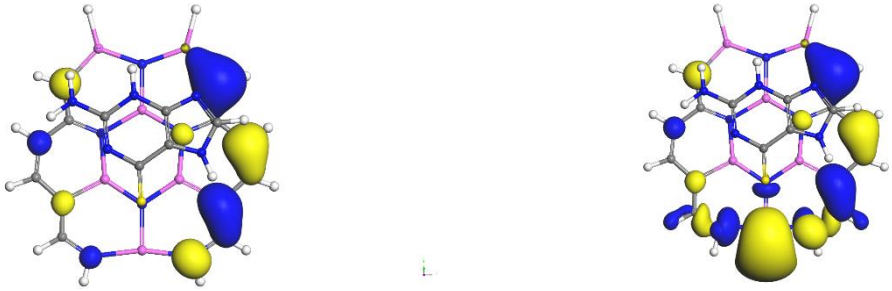

(g) 6-TG/$C_{12}H_{12}N_6AL_6$

Figure 6 : HOMO and LUMO maps of the complexes (6-TG+Coronene) (a) 6-TG/$C_{24}H_{12}$ (b) 6-TG/$C_{12}H_{12}B_6N_6$ (c) 6-TG/ $H_{12}B_{12}N_{12}$ (d)6-TG/$C_{12}H_8B_6N_6P_4$ and (e) 6-TG/$B_{12}N_{12}P_{12}$ (f) 6-TG / $H_{12}N_{12}AL_{12}$ (g) 6-TG/$C_{12}H_{12}N_6AL_6$.

HOMO LOMO

(a) 6-MP/$C_{24}H_{12}$

(b)6-MP/$C_{12}H_{12}B_6N_6$

(c) 6-MP/$H_{12}B_{12}N_{12}$

(d)6-MP/$C_{12}H_8B_6N_6P_4$

(e)6-MP/$B_{12}N_{12}P_{12}$

(f) 6-Mp/$H_{12}N_{12}AL_{12}$

(g) 6-MP/$C_{12}H_{12}N_6AL_6$.

Figure 7 : HOMO and LUMO maps of the complexes (6-MP+Coronene) (a) 6-MP/$C_{24}H_{12}$ (b) 6-MP/$C_{12}H_{12}B_6N_6$ (c) 6-MP/ $H_{12}B_{12}N_{12}$ (d)6-MP/ $C_{12}H_8B_6N_6P_4$ and (e) 6-MP/$B_{12}N_{12}P_{12}$ (f) 6-Mp / $H_{12}N_{12}AL_{12}$ (g) 6-MP/$C_{12}H_{12}N_6AL_6$.

Figures 5 through 7 display the HOMO and LUMO isosurfaces for the respective complexes of the three anticancer drugs with pristine and doped coronene derivatives. These visualizations enable a comparative understanding of how structural modifications influence electronic activity and the drug-nanocarrier interaction profile.

The examination of the HOMO–LUMO Gap (Eg) has uncovered some fascinating insights into the electronic characteristics of various complexes involving 5-Fluorouracil (5-FU), 6-thioguanine (6-TG), and 6-mercaptopurine (6-MP).

	Air Media				Water media			
Structures	E_{HUMO}	E_{LUMO}	E_g	**D.M.**	E_{HUMO}	E_{LUMO}	E_g	**D.M.**
$C_{24}H_{12}$	-5.302	-2.438	2.864	0.000	-5.471	-2.600	2.871	0.005
$H_{12}B_{12}N_{12}$	-6.502	-1.216	5.286	0.000	-6.557	-1.332	5.225	0.067
$C_{12}H_{12}B_6N_6$	-5.100	-2.740	2.360	5.929	-5.230	-2.856	2.374	13.129
$B_{12}N_{12}P_{12}$	-4.254	-4.053	0.201	0.017	-4.306	-4.010	0.296	0.028
$C_{12}H_8B_6N_6P_4$	-4.776	-3.952	0.824	2.234	-4.855	-3.910	0.945	7.561
$H_{12}N_{12}AL_{12}$	-6.482	-1.944	4.538	0.004	-6.393	-1.863	4.530	0.137
$C_{12}H_{12}$ N_6 AL_6	-4.868	-3.421	1.447	4.339	-4.935	-3.403	1.532	9.326
5-FU	-6.311	-2.521	3.790	2.926	-6.132	-2.308	3.824	4.608
5-FU/$C_{24}H_{12}$	-5.329	-2.474	2.855	1.782	-5.426	-2.559	2.867	3.846
5-FU/$H_{12}B_{12}N_{12}$	-6.121	-2.282	3.839	1.939	-6.162	-2.303	3.859	4.131
5-FU/$C_{12}H_{12}B_6N_6$	-5.146	-2.792	2.354	4.137	-6.162	-2.303	3.859	9.250
5-FU/$B_{12}N_{12}P_{12}$	-4.491	-4.317	0.174	1.826	-4.379	-4.100	0.279	3.825
5-FU/$C_{12}H_8B_6N_6P_4$	-4.830	-3.980	0.850	1.272	-4.870	-3.923	0.947	4.100
5-FU/$H_{12}N_{12}AL_{12}$	-6.246	-2.484	3.762	1.689	-6.177	-2.394	3.783	3.108
5-FU/$C_{12}H_{12}N_6AL_6$	-4.879	-3.434	1.445	3.192	-4.930	-3.414	1.516	5.957

Table 4 : HOMO energy (E_{HOMO}), LUMO energy (E_{LUMO}), HOMO–LUMO energy gap (Eg) in (eV) and dipole moment (D.M) in Debye of the complexes (5-FU/Coronene).

In our research centered on the HOMO–LUMO Gap (Eg) for various nanocarrier systems combined with 5-FU, we identified several significant findings. Specifically, the mixture of 5-FU with $B_{12}N_{12}P_{12}$ shows the least energy gap: 0.174 eV in air and 0.279 eV in water. The results illustrate an interesting interaction between 5-FU and different nanocarrier types. When assessing the possibility for electronic reactivity, a significant reduction in the energy gap is observed, indicating that 5-FU is likely to have more effective interactions with its nanocarrier. This could result in improved drug binding and a general enhancement in delivering the drug to its intended target. In contrast, when 5-FU is combined with $H_{12}B_{12}N_{12}$, there is a marked increase in the energy gap, recorded at 3.839 eV in air and 3.859 eV in water. This suggests a decline in electronic reactivity, leading to weaker interactions and potentially less effective binding. Likewise, when 5-FU is associated with $C_{12}H_{12}B_6N_6$, an even greater energy gap of 2.354 eV in air and 3.859 eV in water is observed. This further emphasizes the relatively weaker interactions related to 5-FU. Ultimately, these findings highlight the necessity of choosing an appropriate nanocarrier to improve the delivery and effectiveness of 5-FU. In terms of the Dipole Moment (D.M.), the combination of 5-FU and $B_{12}N_{12}P_{12}$ demonstrates a low dipole moment of 1.8256 Debye in air and 3.8246 Debye in water. This indicates that electronic factors are mainly driving the interaction, leading to reduced polar effects. When 5-FU is combined with $C_{12}H_{12}B_6N_6$, it produces a greater dipole moment of 4.1367 Debye in air and 9.2504 Debye in water, signifying more significant polar interactions. Nevertheless, the larger energy gap implies that the overall efficacy of this interaction for drug delivery is not as favorable when compared to $B_{12}N_{12}P_{12}$.In comparison, when 5-FU is paired with $C_{12}H_{12}B_6N_6$, it yields a higher dipole moment of 4.1367 Debye in air and 9.2504 Debye in water, indicating more substantial polar interactions. However, the wider energy gap suggests that the overall effectiveness of this interaction for drug delivery is less favorable compared to $B_{12}N_{12}P_{12}$.

	Air Media				Water media			
Structures	E_{HUMO}	E_{LUMO}	E_g	**D.M.**	E_{HUMO}	E_{LUMO}	E_g	**D.M.**
$C_{24}H_{12}$	-5.302	-2.438	2.864	0.000	-5.471	-2.600	2.871	0.005
$H_{12}B_{12}N_{12}$	-6.502	-1.216	5.286	0.000	-6.557	-1.332	5.225	0.067
$C_{12}H_{12}B_6N_6$	-5.100	-2.740	2.360	5.929	-5.230	-2.856	2.374	13.129
$B_{12}N_{12}P_{12}$	-4.254	-4.053	0.201	0.017	-4.306	-4.010	0.296	0.028
$C_{12}H_8B_6N_6P_4$	-4.776	-3.952	0.824	2.234	-4.855	-3.910	0.945	7.561
$H_{12}N_{12}AL_{12}$	-6.482	-1.944	4.538	0.004	-6.393	-1.863	4.530	0.137
$C_{12}H_{12}$ N_6 AL_6	-4.868	-3.421	1.447	4.339	-4.935	-3.403	1.532	9.326
6-TG	-5.536	-2.543	2.993	2.742	-5.625	-2.594	3.031	6.010
6-TG/$C_{24}H_{12}$	-5.196	-2.361	2.835	2.173	-5.327	-2.481	2.846	4.876
6-TG/$H_{12}B_{12}N_{12}$	-5.625	-2.281	3.344	1.639	-5.673	-2.364	3.309	3.911
6-TG/$C_{12}H_{12}B_6N_6$	-4.975	-2.632	2.343	6.558	-5.076	-2.720	2.356	16.046
6-TG/$B_{12}N_{12}P_{12}$	-4.210	-4.020	0.190	1.978	-4.299	-4.039	0.260	3.832
6-TG/$C_{12}H_8B_6N_6P_4$	-3.875	-3.051	0.824	1.162	-3.848	-3.038	0.810	5.906
6-TG/$H_{12}N_{12}AL_{12}$	-5.916	-2.611	3.305	0.758	-5.816	-2.540	3.276	3.092
6-TG/$C_{12}H_{12}N_6AL_6$	-4.759	-3.600	1.159	3.393	-4.807	-3.301	1.506	6.220

Table 5 : HOMO energy (E_{HOMO}), LUMO energy (E_{LUMO}), HOMO–LUMO energy gap (Eg) in (eV) and dipole moment (D.M) in Debye of the complexes (6-TG/Coronene).

For 6-TG, the combination with $B_{12}N_{12}P_{12}$ presents the smallest Eg (0.190 eV in air and 0.260 eV in water), reflecting high electronic reactivity and stronger connections between 6-TG and this nanocarrier. This narrow band gap promotes effective electron transfer, improving drug adsorption and delivery. In contrast, combinations such as 6-TG with $H_{12}B_{12}N_{12}$ and $H_{12}N_2AL_{12}$ show larger Eg values (3.344 eV and 3.305 eV in air, respectively), which imply lower reactivity and weaker binding potential. The 6-TG / $C_{12}H_{12}B_6N_6$ complex has a moderate Eg (2.343 eV in air and 2.356 eV in water), indicating somewhat better interactions than the previous combinations but still weaker than with $B_{12}N_{12}P_{12}$. The dipole moment for the 6-TG / $B_{12}N_{12}P_{12}$ pairing is relatively low (1.9777 Debye in air and 3.8315 Debye in water), signifying an interaction driven by electronic factors. Conversely, the 6-TG / $C_{12}H_{12}B_6N_6$ pairing exhibits the highest dipole moment (6.5582

Debye in air and 16.046 Debye in water), indicating stronger polar interactions, yet the larger Eg limits its effectiveness compared to $B_{12}N_{12}P_{12}$.

	Air Media				Water media			
Structures	E_{HUMO}	E_{LUMO}	E_g	**D.M.**	E_{HUMO}	E_{LUMO}	E_g	**D.M.**
$C_{24}H_{12}$	-5.302	-2.438	2.864	0.000	-5.471	-2.600	2.871	0.005
$H_{12}B_{12}N_{12}$	-6.502	-1.216	5.286	0.000	-6.557	-1.332	5.225	0.067
$C_{12}H_{12}B_6N_6$	-5.100	-2.740	2.360	5.929	-5.230	-2.856	2.374	13.129
$B_{12}N_{12}P_{12}$	-4.254	-4.053	0.201	0.017	-4.306	-4.010	0.296	0.028
$C_{12}H_8B_6N_6P_4$	-4.776	-3.952	0.824	2.234	-4.855	-3.910	0.945	7.561
$H_{12}N_{12}AL_{12}$	-6.482	-1.944	4.538	0.004	-6.393	-1.863	4.530	0.137
$C_{12}H_{12}$ N_6 AL_6	-4.868	-3.421	1.447	4.339	-4.935	-3.403	1.532	9.326
6-MP	-5.770	-2.873	2.897	2.641	-5.863	-2.872	2.991	5.008
6-MP/$C_{24}H_{12}$	-5.283	-2.463	2.820	1.622	-5.403	-2.568	2.835	3.430
6-MP/$H_{12}B_{12}N_{12}$	-5.687	-2.481	3.206	1.278	-5.710	-2.522	3.188	3.265
6-MP/$C_{12}H_{12}B_6N_6$	-5.025	-2.694	2.331	6.324	-5.124	-2.778	2.346	14.684
6-MP/$B_{12}N_{12}P_{12}$	-4.266	-4.084	0.182	0.966	-4.339	-4.068	0.271	2.936
6-MP/$C_{12}H_8B_6N_6P_4$	-3.945	-3.122	0.823	2.717	-4.820	-3.895	0.925	8.640
6-MP/$H_{12}N_{12}AL_{12}$	-5.948	-2.770	3.178	1.221	-5.867	-2.709	3.158	2.934
6-MP/$C_{12}H_{12}N_6AL_6$	-4.819	-3.417	1.402	4.369	-4.887	-3.380	1.507	9.461

Table 6 : HOMO energy (E_{HOMO}), LUMO energy (E_{LUMO}), HOMO–LUMO energy gap (Eg) in (eV) and dipole moment (D.M) in Debye of the complexes (6-MP/Coronene).

For 6-MP, the $B_{12}N_{12}P_{12}$ complex shows a small Eg (0.211 eV in air and 0.284 eV in water), denoting strong electronic reactivity and interaction. When paired with $H_{12}B_{12}N_{12}$ and $H_{12}N_{12}AL_{12}$, larger Eg values (3.382 eV and 3.287 eV, respectively) reflect weakened interactions and decreased drug delivery effectiveness. The 6-MP / $C_{12}H_{12}B_6N_6$ complex has a moderate Eg (2.351 eV in air and 2.365 eV in water), indicating more effective interactions than the other two but still not as advantageous as $B_{12}N_{12}P_{12}$. Regarding the Dipole Moment (D.M.), the low dipole moment of 6-MP / $B_{12}N_{12}P_{12}$ (2.0081 Debye in air and 3.8548 Debye in water) suggests low polarity. In comparison, 6-MP / $C_{12}H_{12}B_6N_6$ shows the highest dipole moment values of all the systems

analyzed, recording 6.6294 Debye in air and 16.122 Debye in water; however, its larger Eg limits its effectiveness compared to $B_{12}N_{12}P_{12}$.

To sum up, among all the complexes examined for 5-FU, 6-TG, and 6-MP, $B_{12}N_{12}P_{12}$ emerges as the most promising option for drug delivery.

4.4 DOS Spectra

The Density of States (DOS) and Projected Density of States (PDOS) spectra are essential tools for analyzing the electronic structure of systems that integrate drugs with nanocarriers. In essence, the DOS reveals the distribution of electronic states within the nanomaterial, whereas the PDOS provides information about the specific contributions from individual atoms or orbitals in that system. The DOS aids in understanding the general electronic behavior of the nanocarrier and how drug adsorption influences that behavior. Conversely, the PDOS offers a more detailed analysis, emphasizing the roles of specific atoms—such as carbon, boron, nitrogen, or phosphorus in determining the electronic states of the nanocarrier and how the drug alters this distribution. When interpreting the DOS and PDOS plots, we used a dual color coding system: The blue color represents the total DOS for the system as a whole, which includes the anticancer drug (like 5-FU, 6-TG, or 6-MP) interacting with the surface of the nanosheet (for example, $C_{24}H_{12}$, $C_{12}H_{12}B_6N_6$, and so on). This illustrates the electronic behavior of the complete hybrid system after the drug has been absorbed. In contrast, the red color represents the density of states (DOS) contributions that originate exclusively from the drug molecule. This reveals how the electronic states of the drug interact with and affect the overall DOS of the entire system. This distinction enables us to understand not only the collective behavior of the drug-nanocarrier system but also the individual contributions from each component.

Figures 8–10 illustrate the Density of States (DOS) and Projected Density of States (PDOS) spectra for both unmodified coronene and its nanosheets that have been infused with three distinct anticancer medications: 5-fluorouracil (5-FU), 6-thioguanine (6-TG), and 6-mercaptopurine (6-MP). For ease of comparison, Table 7 summarizes key quantitative parameters derived from the DOS and PDOS analyses, including measurements for the band gap, locations of the HOMO–LUMO levels, and changes in the Fermi level. This overview enables us to clearly understand how the addition of each drug influences the electronic characteristics of coronene.

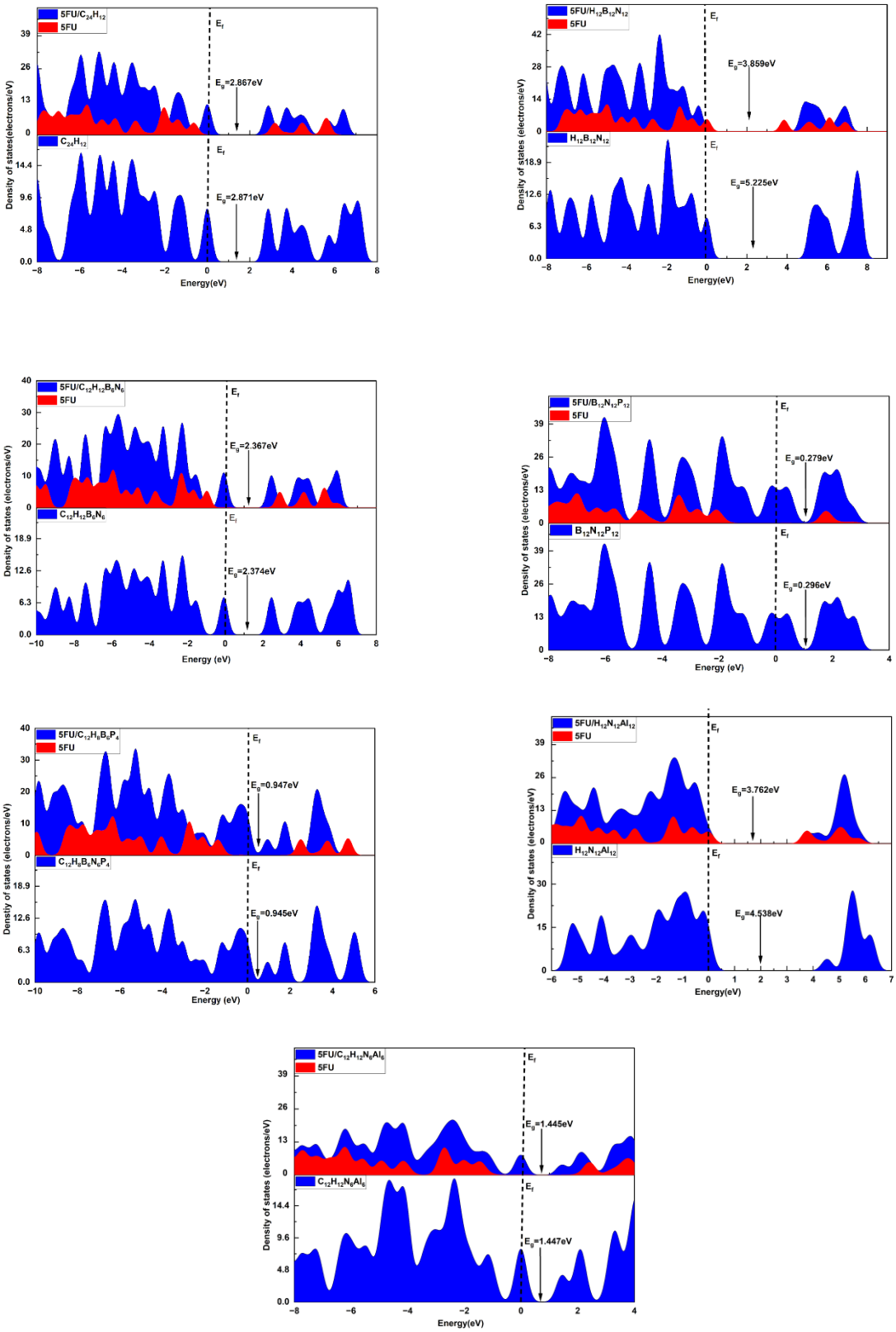

Figure 8 : DOS and PDOS spectra of the coronene and doped nanosheets of (5-FU + Coronene)

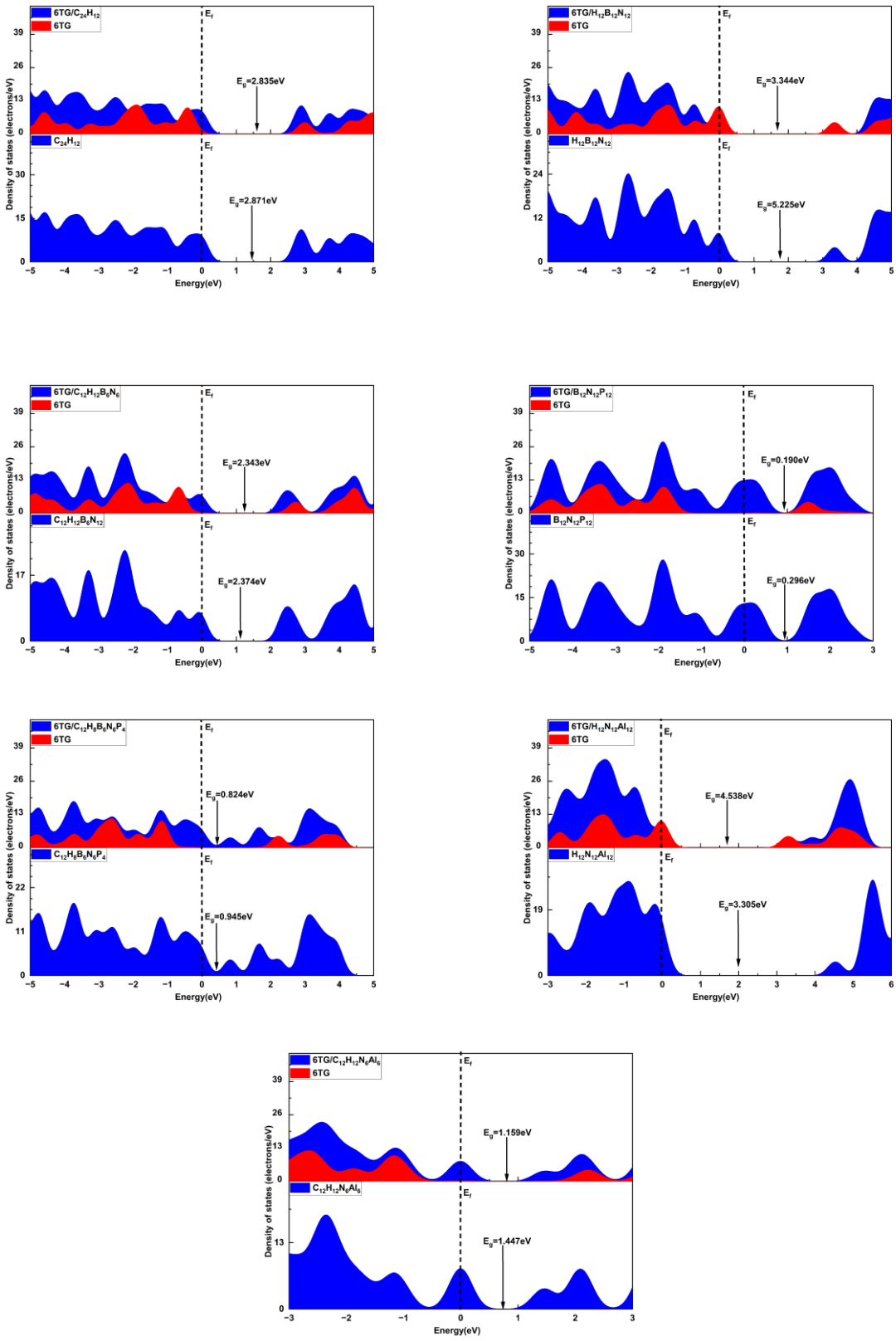

Figure 9 : DOS and PDOS spectra of the coronene and doped nanosheets of (6-TG/Coronene).

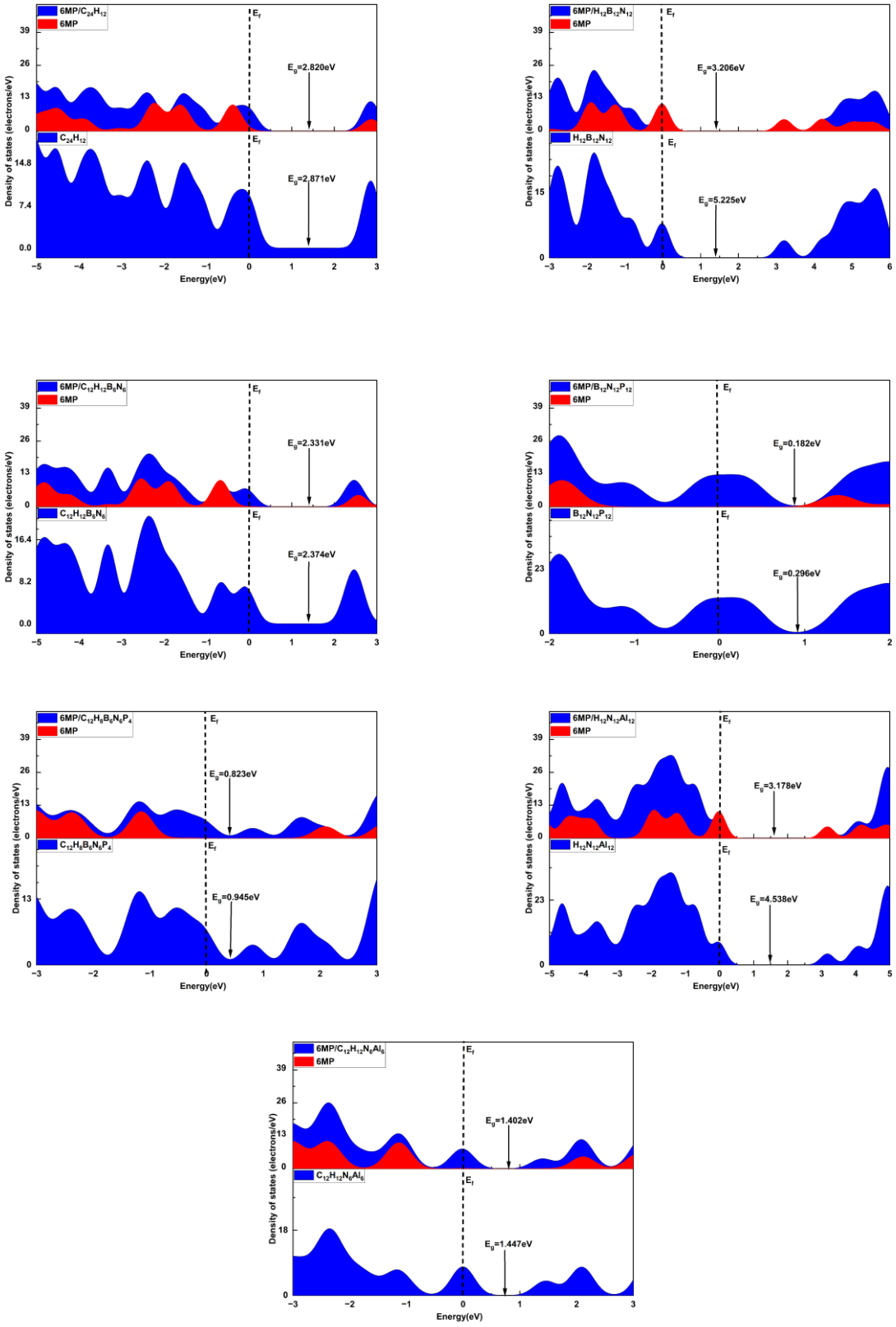

Figure 10 : DOS and PDOS spectra of the coronene and doped nanosheets of (6-MP/Coronene).

structure	Density of states(electrons/eV) E_g-Complex	Eg (eV) – Nanosheet
5-FU/$C_{24}H_{12}$	2.867	2.871
5-FU/$H_{12}B_{12}N_{12}$	3.859	5.225
5-FU/$C_{12}H_{12}B_6N_6$	2.367	2.374
5-FU/$B_{12}N_{12}P_{12}$	0.279	0.296
5-FU/$C_{12}H_8B_6N_6P_4$	0.947	0.945
5-FU/$H_{12}N_{12}AL_{12}$	3.762	4.538
5-FU/$C_{12}H_{12}N_6AL_6$	1.445	1.447
6-TG/$C_{24}H_{12}$	2.835	2.871
6-TG/$H_{12}B_{12}N_{12}$	3.344	5.225
6-TG/$C_{12}H_{12}B_6N_6$	2.343	2.374
6-TG/$B_{12}N_{12}P_{12}$	0.190	0.296
6-TG/$C_{12}H_8B_6N_6P_4$	0.824	0.945
6-TG/$H_{12}N_{12}AL_{12}$	4.538	3.30
6-TG/$C_{12}H_{12}N_6AL_6$	1.159	1.447
6-MP/$C_{24}H_{12}$	2.820	2.871
6-MP/$H_{12}B_{12}N_{12}$	3.206	5.225
6-MP/$C_{12}H_{12}B_6N_6$	2.331	2.374
6-MP/$B_{12}N_{12}P_{12}$	0.182	0.296
6-MP/$C_{12}H_8B_6N_6P_4$	0.823	0.945
6-MP/$H_{12}N_{12}AL_{12}$	3.178	4.538
6-MP/$C_{12}H_{12}N_6AL_6$	1.402	1.447

Table 7 : Generating table from DOS and PDOS spectra of the coronene and doped nanosheets for three anticancer drugs (5-FU, 6-TG, 6-MP).

Among the various systems analyzed, the $B_{12}N_{12}P_{12}$ nanosheet stands out due to its lowest energy gaps post-adsorption when tested with the three anticancer drugs 5-FU, 6-TG, and 6-MP. The nanosheet displays exceptional electronic reactivity, demonstrating energy gaps of just 0.279 eV,

0.190 eV, and 0.182 eV. This suggests it holds significant promise as a drug delivery system. In contrast, the $H_{12}B_{12}N_{12}$ nanosheet shows much larger energy gaps after drug adsorption, with values of 3.859 eV for 5-FU, 3.344 eV for 6-TG, and 3.206 eV for 6-MP. This notable variation emphasizes the distinct characteristics of each nanosheet concerning drug interactions. This indicates that despite its lower conductivity, it possesses improved electronic stability. This stable property may be beneficial for controlled or prolonged drug release. In addition, various doped nanosheets such as $C_{12}H_8B_6N_6P_4$ and $C_{12}H_{12}B_6N_6$ show relatively moderate energy gap values. This indicates a suitable equilibrium between reactivity and stability, making them appealing options for adaptable drug delivery methods that can be tailored to meet particular therapeutic requirements.

4.5 Electronic Structures and Charge Transfer Analysis

The maps depicting electron density (ED) and electrostatic potential (ESP) are vital for illustrating molecular interactions and charge distributions, especially in the context of drug and nanocarrier interactions. Simply put, electron density reveals areas where electrons are most likely found within a molecule, while ESP maps illustrate the electrostatic forces acting on a positive test charge in proximity to that molecule. This distinction allows for the identification of regions dense in electrons compared to those that are electron-deficient. In Figures 11 to 13, the ED maps illustrate the complexes formed by 5-FU, 6-TG, and 6-MP in combination with both pristine and doping-treated coronene-based nanosheets. There is a notable overlap in electron density between the drugs and the surfaces of the nanosheets, indicating robust interactions and charge redistribution that happen when the drugs attach to the nanosheets. This overlap implies the creation of stable complexes, largely attributed to the enhanced electronic delocalization at the interface between the drug and the nanosheet. The presence of denser electron clouds around heteroatoms and in the π-electron-rich areas of the nanosheets indicates that these regions are crucial for the recognition and binding of drug molecules.

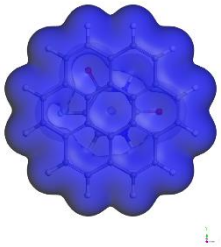

(a) 5-FU/$C_{24}H_{12}$

(b) 5-FU/$B_{12}N_{12}H_{12}$

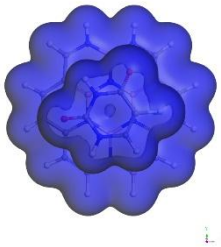

(C)5-FU/$C_{12}H_{12}B_6N_6$

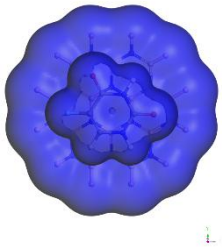

(d) 5-FU/$B_{12}N_{12}P_{12}$

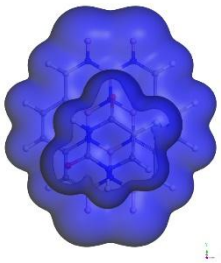

(e) 5-FU/$B_{12}N_{12}H_8P_4$

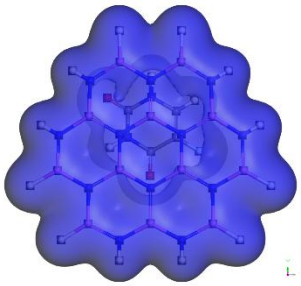

(f) 5-FU/$H_{12}N_{12}AL_{12}$

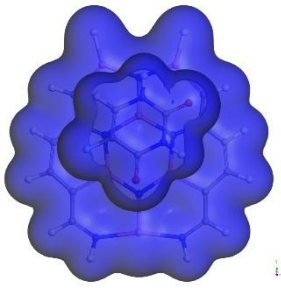

(g) 5-FU/$C_{12}H_{12}N_6AL_6$

Figure 11 : ED maps of the complexes (a) 5-FU/$C_{24}H_{12}$ (b) 5-FU/$B_{12}N_{12}H_{12}$(C) 5-FU/$C_{12}H_{12}B_6N_6$ (d) 5-FU/$B_{12}N_{12}P_{12}$ (e) 5-FU/$B_{12}N_{12}H_8P_4$ (f) 5-FU/$H_{12}N_{12}AL_{12}$ (g) 5-FU/$C_{12}H_{12}N_6AL_6$.

(a) 6-TG/$C_{24}H_{12}$

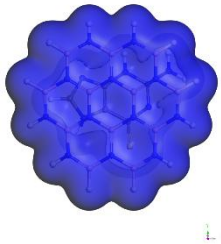

(b) 6-TG/$B_{12}N_{12}H_{12}$

(C) 6-TG/$C_{12}H_{12}B_6N_6$

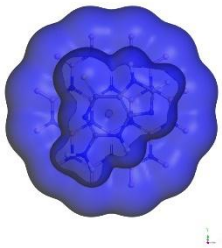

(d) 6-TG/$B_{12}N_{12}P_{12}$

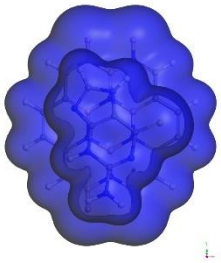

(e) 6-TG/$B_{12}N_{12}H_8P_4$

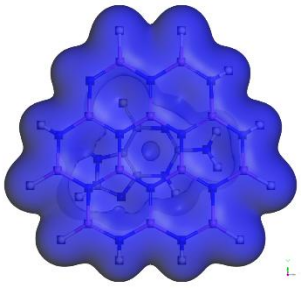

(f) 6-TG/$H_{12}N_{12}AL_{12}$

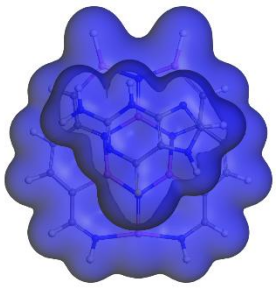

(g) 6-TG/$C_{12}H_{12}N_6AL_6$

Figure 12 : ED maps of the complexes (a) 6-TG/$C_{24}H_{12}$ (b) 6-TG/$B_{12}N_{12}H_{12}$(C) 6-TG / $C_{12}H_{12}B_6N_6$ (d) 6-TG/$B_{12}N_{12}P_{12}$ (e) 6-TG/$B_{12}N_{12}H_8P_4$ (f) 6-TG/$H_{12}N_{12}AL_{12}$ (g) 6-TG /$C_{12}H_{12}N_6AL_6$.

(a) 6-MP/$C_{24}H_{12}$

(b) 6-MP/$B_{12}N_{12}H_{12}$

(C) 6-MP/$C_{12}H_{12}B_6N_6$

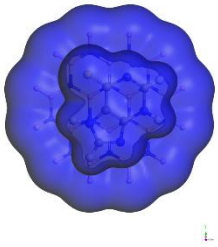

(d) 6-MP/$B_{12}N_{12}P_{12}$

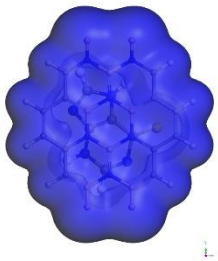

(e) 6-MP/$B_{12}N_{12}H_8P_4$

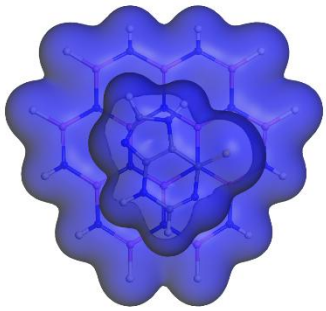

(f) 6-MP/$H_{12}N_{12}AL_{12}$

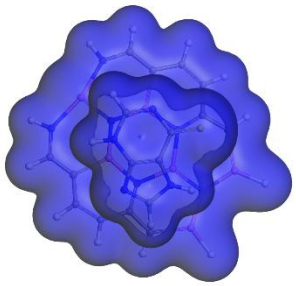

(g) 6-MP/$C_{12}H_{12}N_6AL_6$

Figure 13 : ED maps of the complexes (a) 6-MP/$C_{24}H_{12}$ (b) 6-MP/$B_{12}N_{12}H_{12}$(C) 6-MP/ $C_{12}H_{12}B_6N_6$ (d) 6-MP/$B_{12}N_{12}P_{12}$ (e) 6-MP/$B_{12}N_{12}H_8P_4$ (f) 6-MP/$H_{12}N_{12}AL_{12}$ (g) 6-MP /$C_{12}H_{12}N_6AL_6$.

Looking at Figures 14 to 16, the ESP maps offer a better insight into the complexes established between drugs and nanocarriers. The pink and red areas signify regions with elevated electron density, which are usually linked to electronegative atoms like oxygen and nitrogen present in the drug molecules. These areas are likely involved in electron donation, resulting in a negative charge. Conversely, the violet and blue regions show low electron density, commonly located on the surfaces of the nanosheets or around hydrogen atoms within the drugs, suggesting potential roles as electron-accepting or positively charged regions.

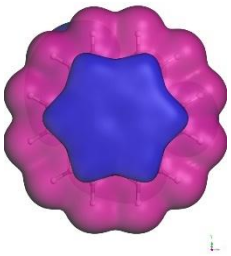

(a) 5-FU/$C_{24}H_{12}$

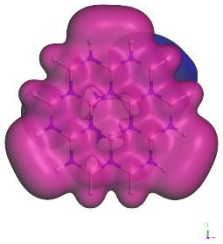

(b) 5-FU/$B_{12}N_{12}H_{12}$

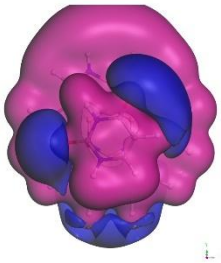

(C)5-FU/$C_{12}H_{12}B_6N_6$

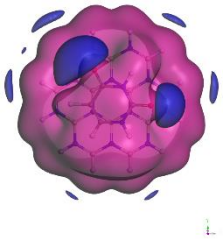

(d) 5-FU/$B_{12}N_{12}P_{12}$

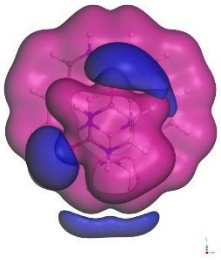

(e) 5-FU/$B_{12}N_{12}H_8P_4$

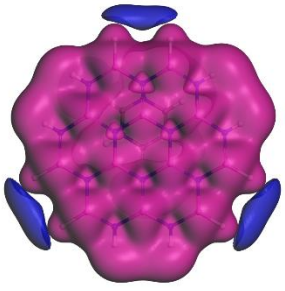

(f) 5-FU/$H_{12}N_{12}AL_{12}$

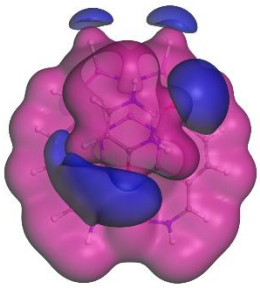

(g) 5-FU/$C_{12}H_{12}N_6AL_6$

Figure 14 : ESP maps of the complexes (a) 5-FU/$C_{24}H_{12}$ (b) 5-FU/$B_{12}N_{12}H_{12}$(C) 5-FU/$C_{12}H_{12}B_6N_6$ (d) 5-FU/$B_{12}N_{12}P_{12}$ (e) 5-FU/$B_{12}N_{12}H_8P_4$ (f) 5-FU/$H_{12}N_{12}AL_{12}$ (g) 5-FU/$C_{12}H_{12}N_6AL_6$.

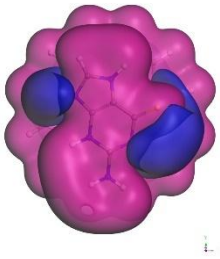

(a) 6-TG/$C_{24}H_{12}$

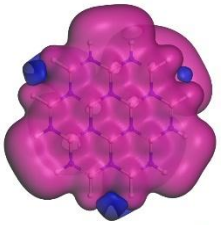

(b) 6-TG/$B_{12}N_{12}H_{12}$

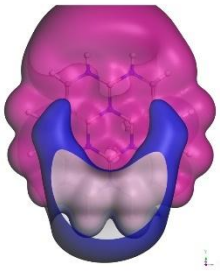

(C) 6-TG/$C_{12}H_{12}B_6N_6$

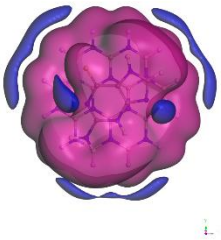

(d) 6-TG/$B_{12}N_{12}P_{12}$

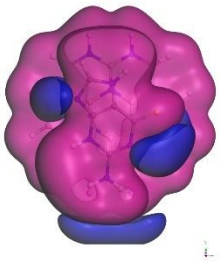

(e) 6-TG/$B_{12}N_{12}H_8P_4$

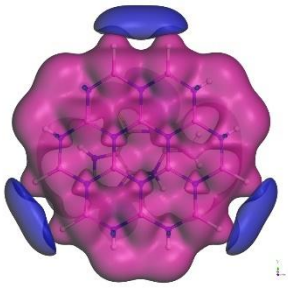

(f) 6-TG/$H_{12}N_{12}AL_{12}$

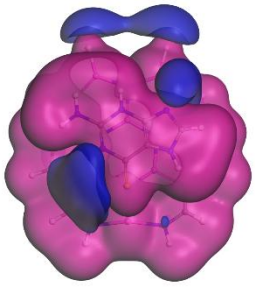

(g) 6-TG/$C_{12}H_{12}N_6AL_6$

Figure 15 : ESP maps of the complexes (a) 6-TG/$C_{24}H_{12}$ (b) 6-TG / $B_{12}N_{12}H_{12}$(C) 6-TG/ $C_{12}H_{12}B_6N_6$ (d) 6-TG/$B_{12}N_{12}P_{12}$ (e) 6-TG/$B_{12}N_{12}H_8P_4$ (f) 6-TG/$H_{12}N_{12}AL_{12}$ (g) 6-TG /$C_{12}H_{12}N_6AL_6$.

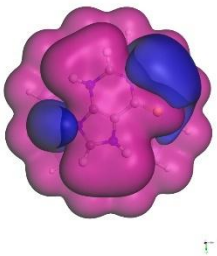

(a) 6-MP/$C_{24}H_{12}$

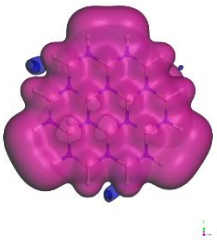

(b) 6-MP/$B_{12}N_{12}H_{12}$

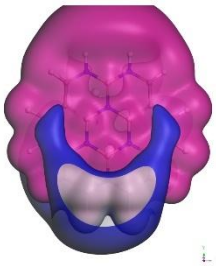

(C) 6-MP/$C_{12}H_{12}B_6N_6$

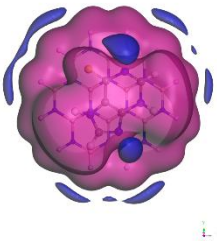

(d) 6-MP/$B_{12}N_{12}P_{12}$

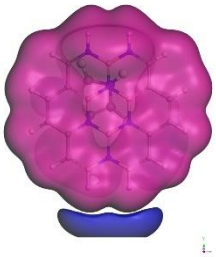

(e) 6-MP/$B_{12}N_{12}H_8P_4$

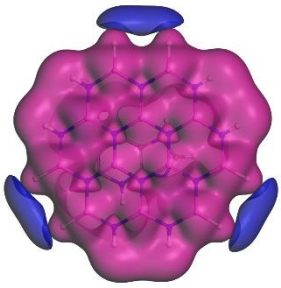

(f) 6-MP/$H_{12}N_{12}AL_{12}$

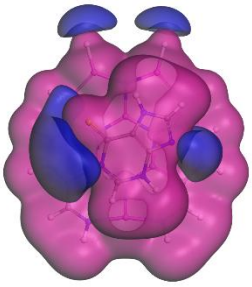

(g) 6-MP/$C_{12}H_{12}N_6AL_6$

Figure 16 : ESP maps of the complexes (a) 6-MP/$C_{24}H_{12}$ (b) 6-MP / $B_{12}N_{12}H_{12}$(C) 6-MP/ $C_{12}H_{12}B_6N_6$ (d) 6-MP/$B_{12}N_{12}P_{12}$ (e) 6-MP/$B_{12}N_{12}H_8P_4$ (f) 6-MP/$H_{12}N_{12}AL_{12}$ (g) 6-MP /$C_{12}H_{12}N_6AL_6$.

In conclusion, the examination of both ED and ESP provides a more thorough understanding of how drugs interact with nanosheets via electrostatic forces and orbital overlap. These interactions are significantly affected by local charge distribution and surface characteristics. Gaining these insights is essential for comprehending how drugs are taken up by nanocarriers, which directly influences their loading, release, and overall therapeutic effectiveness.

4.6 Dipole Moment Analysis

The dipole moment is an important concept that helps in grasping the electronic characteristics of molecules, offering understanding into their charge distribution, polarity, and reactivity. A molecule that is generally seen as non-polar has a dipole moment close to zero, whereas a larger dipole moment signifies a notable charge imbalance, leading to more intense interactions with polar solvents like water. Therefore, analyzing dipole moments is vital for understanding electron distribution as well as aspects such as solubility, bioavailability, and reactivity, particularly regarding drug delivery systems. This research examined the dipole moments of unmodified coronene ($C_{24}H_{12}$) along with various derivatives modified with heteroatoms. They investigated

how these changes influence interactions with three anticancer drugs: 5-fluorouracil (5-FU), 6-thioguanine (6-TG), and 6-mercaptopurine (6-MP). The results were illustrated using blue bars for air measurements and orange bars for measurements taken in water, clearly demonstrating the impact of water on polarization in figure 17.

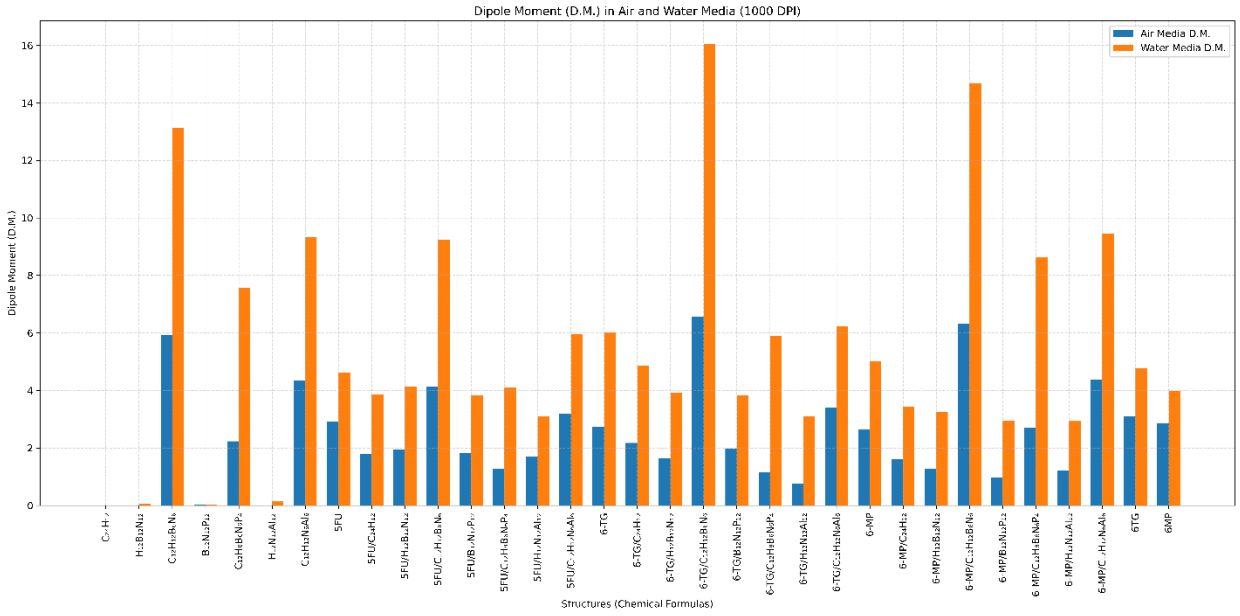

Figure 17 : Comparison of the dipole moments (in Debye) of pristine doped coronene nanosheets and their respective drug-loaded complexes (5-FU, 6-TG, and 6-MP) between the cases in the air and in water media before and after adsorption.

The investigation showed that pristine coronene has an extremely low dipole moment (0.0004 D in air and 0.0046 D in water) due to its symmetrical configuration. However, the addition of heteroatoms like boron (B), nitrogen (N), phosphorus (P), or aluminum (Al) disrupts this symmetry, leading to higher dipole moments. For instance, the derivative $C_{12}H_{12}B_6N_6$ exhibits a dipole moment of 5.9291 D in air, whereas $C_{12}H_{12}N_6Al_6$ shows a dipole moment of 4.3387 D. Moreover, when drugs are adsorbed onto these modified structures, their dipole moments increase even further, especially in systems containing combinations of B, N, and P. The highest dipole moment recorded in air was found in the complex of 6-TG with $C_{12}H_{12}B_6N_6$, reaching 6.5582 D, closely followed by the complex with 6-MP at 6.3244 D, demonstrating the significant charge redistribution that happens during drug binding. In water, dipole moments become even more significant due to the effects of solvent polarization. The greatest dipole moments recorded in this

environment were for the combinations of 6-TG and $C_{12}H_{12}B_6N_6$ at 16.046 D and 6-MP and $C_{12}H_{12}B_6N_6$ at 14.684 D, indicating strong electrostatic interactions between the drug molecules and the doped coronene nanosheets.

The research indicates that the combination of B–N doping with drug adsorption significantly enhances the dipole moment, particularly in aqueous conditions, by improving charge separation and increasing solvent polarization. These findings emphasize the potential of $C_{12}H_{12}B_6N_6$-based coronene nanosheets for use in drug delivery and sensing within biological systems, where strong electrostatic interactions may enhance stability and overall effectiveness.

4.7 Quantum Molecular Descriptors

The detailed quantum chemical analysis across pristine nanosheets, individual drugs, and their complexes with 5-FU, 6-TG, and 6-MP provides significant insights into their electronic behavior, reactivity, and interaction tendencies in both gas and aqueous media.

Structure	**Gas Media**					**Water Media**				
	μ	**η**	**s**	**ω**	**ν**	**μ**	**η**	**s**	**ω**	**ν**
$C_{24}H_{12}$	3.870	1.432	0.349	5.229	0.191	4.036	1.436	0.348	5.672	0.176
$H_{12}B_{12}N_{12}$	3.859	2.643	0.189	2.817	0.355	3.945	2.613	0.191	2.978	0.336
$C_{12}H_{12}B_6N_6$	3.920	1.180	0.424	6.511	0.154	4.043	1.187	0.421	6.885	0.145
$B_{12}N_{12}P_{12}$	4.154	0.101	4.975	85.829	0.012	4.158	0.148	3.378	58.409	0.017
$C_{12}H_8B_6N_6P_4$	4.364	0.412	1.214	23.112	0.043	4.383	0.473	1.058	20.324	0.049
$H_{12}N_{12}AL_{12}$	4.213	2.269	0.220	3.911	0.256	4.128	2.265	0.221	3.762	0.266
$C_{12}H_{12}N_6AL_6$	4.145	0.724	0.691	11.871	0.084	4.169	0.766	0.653	11.345	0.088

Table 8 : Global hardness, Global softness, Chemical potential, Electrophilicity index and Nucleophilicity index Calculations.

Structure	Gas Media					Water Media				
	μ	η	s	ω	ν	μ	η	s	ω	ν
$C_{24}H_{12}$	3.870	1.432	0.349	5.229	0.191	4.036	1.436	0.348	5.672	0.176
$H_{12}B_{12}N_{12}$	3.859	2.643	0.189	2.817	0.355	3.945	2.613	0.191	2.978	0.336
$C_{12}H_{12}B_6N_6$	3.920	1.180	0.424	6.511	0.154	4.043	1.187	0.421	6.885	0.145
$B_{12}N_{12}P_{12}$	4.154	0.101	4.975	85.829	0.012	4.158	0.148	3.378	58.409	0.017
$C_{12}H_8B_6N_6P_4$	4.364	0.412	1.214	23.112	0.043	4.383	0.473	1.058	20.324	0.049
$H_{12}N_{12}AL_{12}$	4.213	2.269	0.220	3.911	0.256	4.128	2.265	0.221	3.762	0.266
$C_{12}H_{12}N_6AL_6$	4.145	0.724	0.691	11.871	0.084	4.169	0.766	0.653	11.345	0.088
5-FU	4.416	1.895	0.264	5.145	0.194	4.220	1.912	0.262	4.657	0.215
5-FU/$C_{24}H_{12}$	3.902	1.428	0.350	5.332	0.188	3.993	1.434	0.349	5.560	0.180
5-FU/ $H_{12}B_{12}N_{12}$	4.202	1.920	0.261	4.598	0.218	4.233	1.930	0.259	4.642	0.215
5-FU/$C_{12}H_{12}B_6N_6$	3.969	1.177	0.425	6.692	0.149	4.233	1.930	0.259	4.642	0.215
5-FU/$B_{12}N_{12}P_{12}$	4.404	0.087	5.747	111.467	0.009	4.240	0.140	3.584	64.421	0.016
5-FU/ $C_{12}H_8B_6N_6P_4$	4.405	0.425	1.177	22.828	0.044	4.397	0.474	1.056	20.411	0.049
5-FU/ $H_{12}N_{12}AL_{12}$	4.365	1.881	0.266	5.065	0.197	4.286	1.892	0.264	4.855	0.206
5-FU/$C_{12}H_{12}N_6AL_6$	4.157	0.723	0.692	11.956	0.084	4.172	0.758	0.660	11.481	0.087

Table 9 :Global hardness, Global softness, Chemical potential, Electrophilicity index and Nucleophilicity index Calculations for (nanosheets and 5-FU complexes)

Structure	Gas Media					Water Media				
	μ	η	s	ω	ν	μ	η	s	ω	ν
$C_{24}H_{12}$	3.870	1.432	0.349	5.229	0.191	4.036	1.436	0.348	5.672	0.176
$H_{12}B_{12}N_{12}$	3.859	2.643	0.189	2.817	0.355	3.945	2.613	0.191	2.978	0.336
$C_{12}H_{12}B_6N_6$	3.920	1.180	0.424	6.511	0.154	4.043	1.187	0.421	6.885	0.145
$B_{12}N_{12}P_{12}$	4.154	0.101	4.975	85.829	0.012	4.158	0.148	3.378	58.409	0.017
$C_{12}H_8B_6N_6P_4$	4.364	0.412	1.214	23.112	0.043	4.383	0.473	1.058	20.324	0.049
$H_{12}N_{12}AL_{12}$	4.213	2.269	0.220	3.911	0.256	4.128	2.265	0.221	3.762	0.266
$C_{12}H_{12}N_6AL_6$	4.145	0.724	0.691	11.871	0.084	4.169	0.766	0.653	11.345	0.088
6-TG	4.040	1.497	0.334	5.452	0.183	4.110	1.516	0.330	5.572	0.180
6-TG/$C_{24}H_{12}$	3.779	1.418	0.353	5.036	3.779	3.904	1.423	0.351	5.355	0.187

6-TG / $H_{12}B_{12}N_{12}$	4.040	1.497	0.334	5.452	0.183	4.019	1.655	0.302	4.880	0.205
6-TG/$C_{12}H_{12}B_6N_6$	3.953	1.672	0.299	4.673	0.214	3.898	1.178	0.424	6.449	0.155
6-TG /$B_{12}N_{12}P_{12}$	3.804	1.172	0.427	6.174	0.162	4.169	0.130	3.846	66.848	0.015
6TG/$C_{12}H_8B_6N_6P_4$	4.115	0.095	5.263	89.122	0.011	3.443	0.405	1.235	14.635	0.068
6-TG /$H_{12}N_{12}AL_{12}$	3.463	0.412	1.214	14.554	0.069	4.178	1.638	0.305	5.328	0.188
6TG/$C_{12}H_{12}N_6AL_6$	4.264	1.653	0.303	5.500	0.182	4.054	0.753	0.664	10.913	0.092

Table 10 : Global hardness, Global softness, Chemical potential, Electrophilicity index and Nucleophilicity index Calculations for (nanosheets and 6-TG complexes).

Structure	**Gas Media**					**Water Media**				
	μ	**η**	**s**	**ω**	**ν**	**μ**	**η**	**s**	**ω**	**ν**
$C_{24}H_{12}$	3.870	1.432	0.349	5.229	0.191	4.036	1.436	0.348	5.672	0.176
$H_{12}B_{12}N_{12}$	3.859	2.643	0.189	2.817	0.355	3.945	2.613	0.191	2.978	0.336
$C_{12}H_{12}B_6N_6$	3.920	1.180	0.424	6.511	0.154	4.043	1.187	0.421	6.885	0.145
$B_{12}N_{12}P_{12}$	4.154	0.101	4.975	85.829	0.012	4.158	0.148	3.378	58.409	0.017
$C_{12}H_8B_6N_6P_4$	4.364	0.412	1.214	23.112	0.043	4.383	0.473	1.058	20.324	0.049
$H_{12}N_{12}AL_{12}$	4.213	2.269	0.220	3.911	0.256	4.128	2.265	0.221	3.762	0.266
$C_{12}H_{12}$ N_6 AL_6	4.145	0.724	0.691	11.871	0.084	4.169	0.766	0.653	11.345	0.088
6-MP	1.449	0.345	6.446	0.155	1.449	4.368	1.496	0.334	6.378	0.157
6-MP/$C_{24}H_{12}$	1.410	0.355	5.319	0.188	1.410	3.986	1.418	0.353	5.603	0.179
6-MP/$H_{12}B_{12}N_{12}$	1.603	0.312	5.203	0.192	1.603	4.116	1.594	0.314	5.314	0.188
6-MP/$C_{12}H_{12}B_6N_6$	1.166	0.429	6.390	0.157	1.166	3.951	1.173	0.426	6.654	0.150
6-MP/$B_{12}N_{12}P_{12}$	0.091	5.495	95.773	0.010	0.091	4.204	0.136	3.690	65.201	0.015
6MP/$C_{12}H_8B_6N_6P_4$	0.412	1.215	15.171	0.066	0.412	4.358	0.463	1.081	20.527	0.049
6-MP/$H_{12}N_{12}AL_{12}$	1.589	0.315	5.979	0.167	1.589	4.288	1.579	0.317	5.822	0.172
6MP/$C_{12}H_{12}N_6AL_6$	0.701	0.713	12.096	0.083	0.701	4.134	0.754	0.664	11.338	0.088

Table 11: Global hardness, Global softness, Chemical potential, Electrophilicity index and Nucleophilicity index Calculations for (nanosheets and 6-MP complexes).

Across all systems, the aqueous phase results in consistent changes to descriptor values. In particular: Hardness (η) tends to decrease in water, indicating enhanced electronic softness and

polarizability, which favors interactions in biological environments. Chemical potential (μ) remains relatively stable across media, but slight variations influence the resulting electrophilic and nucleophilic indices. Softness (s) increases in water, highlighting a greater susceptibility to charge transfer, making these complexes more reactive in polar biological systems.The electrophilicity index (ω) and nucleophilicity index (υ) show inverse trends, providing a clear view of whether the material behaves more as an electron acceptor (electrophile) or donor (nucleophile). $B_{12}N_{12}P_{12}$ and $C_{12}H_8B_6N_6P_4$ complexes exhibit exceptionally high ω values (up to 111.47 in gas and 97.56 in water), making them strong electrophilic carriers, ideal for interacting with nucleophilic drug moieties. In contrast, $C_{24}H_{12}$ and $H_{12}B_{12}N_{12}$ show moderate ω values and high υ, making them suitable for balanced charge transfer interactions, potentially enabling controlled drug delivery. The electronic descriptors of 5-FU, 6-TG, and 6-MP loaded onto the same nanosheets (e.g., $B_{12}N_{12}P_{12}$ or $C_{12}H_8B_6N_6P_4$) remain almost identical, suggesting that the carrier's composition dictates the electronic properties more strongly than the drug. However, slight variations in μ and η still affect ω and υ, indicating subtle differences in how each drug modifies the carrier's interaction capacity.

Highest Electrophilicity has show among these complexes 5-FU/$B_{12}N_{12}P_{12}$ and 6-MP/$B_{12}N_{12}P_{12}$ in gas phase (ω ≈ 111.467), 5-FU/$H_{12}B_{12}N_{12}$ and 6-MP/$H_{12}B_{12}N_{12}$ in water phase (ω ≈ 97.56).

And the Highest Nucleophilicity of the complexes has been observed among the complexes such as $C_{12}H_8B_6N_6$, $C_{12}H_{12}B_6N_6$, and $C_{24}H_{12}$ systems (υ ranging from 3.9–5.8), indicating excellent electron-donating ability. A higher ω implies stronger interaction potential, which is favorable for stable drug adsorption but might hinder drug release. Systems with moderate ω and higher softness (s) may offer the best balance between binding strength and reversibility, which is critical for efficient loading and controlled release. Carriers like $C_{12}H_{12}N_6Al_6$ and $H_{12}N_{12}Al_{12}$ maintain stable profiles in both gas and aqueous media, indicating robust reactivity and transferability across environments.

4.8 Solvation Energy

To assess the solvent effect on the adsorption behavior of anticancer drugs (5-FU, 6-TG, and 6-MP) on pristine and doped coronene nanosheets, we performed solvation energy calculations and COSMO surface analyses within an aqueous environment.

The solvation energy (E_{solv}) was calculated as the difference between the total energy of each complex in water and in the gas phase (air) as follows:

$$E_{solv} = E_{water} - E_{air}$$

Negative values of E_{solv} signify enhanced stability and solubility of the complexes in the aqueous phase.

Structures	Solvation energy (eV)
$C_{24}H_{12}$	-0.2541
5-FU	-0.4399
$H_{12}B_{12}N_{12}$	-0.3557
$C_{12}H_{12}B_6N_6$	-0.4136
$B_{12}N_{12}P_{12}$	-0.5627
$C_{12}H_8B_6N_6P_4$	-0.3152
$H_{12}N_{12}AL_{12}$	-0.3186
$C_{12}H_{12}$ N_6 AL_6	-0.3023
5-FU/$C_{24}H_{12}$	-0.5820
5-FU/$H_{12}B_{12}N_{12}$	-0.7100
5-FU/$C_{12}H_{12}B_6N_6$	-0.7302
5-FU/$B_{12}N_{12}P_{12}$	-0.7597
5-FU/$C_{12}H_8B_6N_6P_4$	-0.6102
5-FU/$H_{12}N_{12}AL_{12}$	-0.6116
5-FU/$C_{12}H_{12}N_6AL_6$	-0.6261
6-TG	-0.5637
6-TG/$C_{24}H_{12}$	-0.6431
6-TG/$H_{12}B_{12}N_{12}$	-0.7586
6-TG/$C_{12}H_{12}B_6N_6$	-0.8193
6-TG/$B_{12}N_{12}P_{12}$	-0.8241
6-TG/$C_{12}H_8B_6N_6P_4$	-0.6892
6-TG/$H_{12}N_{12}AL_{12}$	-0.6665
6-TG/$C_{12}H_{12}N_6AL_6$	-0.6783

6-MP	-0.4493
6-MP/$C_{24}H_{12}$	-0.5461
6-MP/$H_{12}B_{12}N_{12}$	-0.6562
6-MP/$C_{12}H_{12}B_6N_6$	-0.7266
6-MP/$B_{12}N_{12}P_{12}$	-0.7516
6-MP/$C_{12}H_8B_6N_6P_4$	-0.6134
6-MP/$H_{12}N_{12}AL_{12}$	-0.6034
6-MP/$C_{12}H_{12}N_6AL_6$	-0.6111

Table 12 : Solvation energy of the nanosheets and complexes.

As presented in Table 12, all drug-nanosheet complexes exhibit negative solvation energies, confirming their favorable stability in water. The solvation energies of the 5-FU complexes range from −0.5819-0.5819−0.5819 eV for 5-FU/$C_{24}H_{12}$ to −0.7597eV for 5-FU/$B_{12}N_{12}P_{12}$ demonstrating improved stability upon nanosheet doping. Similarly, the 6-TG complexes show even stronger solvation effects, with values reaching as low as −0.8241eV for 6-TG/$B_{12}N_{12}P_{12}$. The 6-MP complexes also maintain negative solvation energies indicating good aqueous stability for 6-MP/$B_{12}N_{12}P_{12}$ has a solvation energy of −0.7516eV.

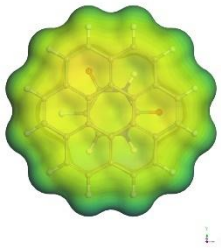

(a) 5-FU/$C_{24}H_{12}$

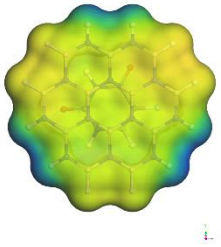

(b) 5-FU/$B_{12}N_{12}H_{12}$

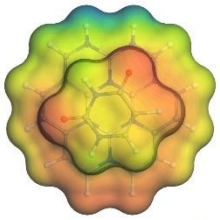

(C)5-FU/$C_{12}H_{12}B_6N_6$

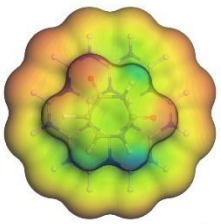

(d) 5-FU/$B_{12}N_{12}P_{12}$

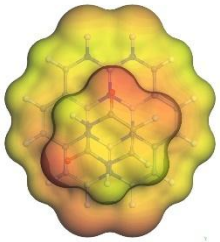

(e) 5-FU/$B_{12}N_{12}H_8P_4$

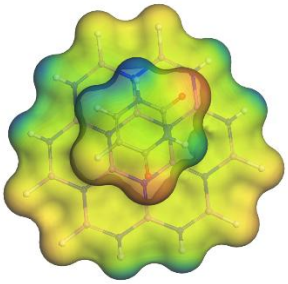

(f) 5-FU/$H_{12}N_{12}AL_{12}$

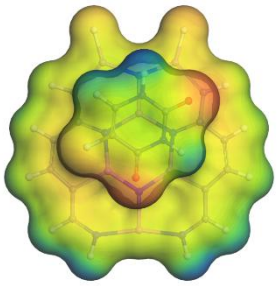

(g) 5-FU/$C_{12}H_{12}N_6AL_6$

Figure 18 : Front views of the COSMO surfaces of the complexes (a) 5-FU/ $C_{24}H_{12}$ (b) 5-FU/ $B_{12}N_{12}H_{12}$(C) 5-FU/$C_{12}H_{12}B_6N_6$ (d) 5-FU/ $B_{12}N_{12}P_{12}$ (e) 5-FU/ $B_{12}N_{12}H_8P_4$ (f) 5-FU/ $H_{12}N_{12}AL_{12}$ (g) 5-FU/$C_{12}H_{12}N_6AL_6$.

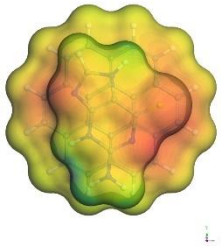

(a) 6-TG/$C_{24}H_{12}$

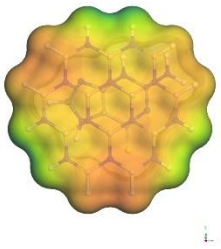

(b) 6-TG/$B_{12}N_{12}H_{12}$

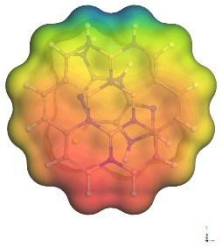

(C) 6-TG/$C_{12}H_{12}B_6N_6$

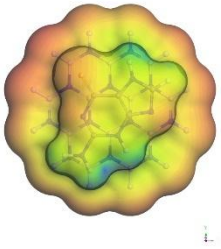

(d) 6-TG/$B_{12}N_{12}P_{12}$

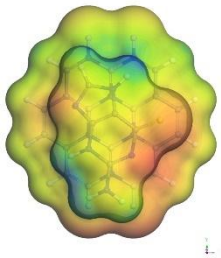

(e) 6-TG/$B_{12}N_{12}H_8P_4$

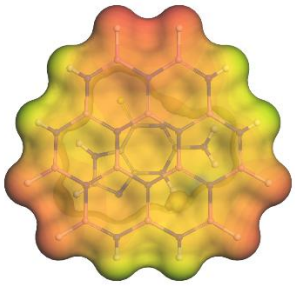

(f) 6-TG/$H_{12}N_{12}AL_{12}$

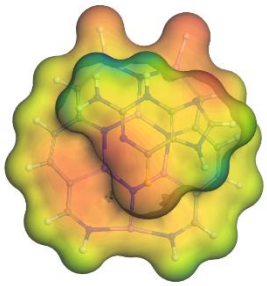

(g) 6-TG/$C_{12}H_{12}N_6AL_6$

Figure 19 **:** Front views of the COSMO surfaces of the complexes (a) 6-TG/$C_{24}H_{12}$ (b) 6-TG/$B_{12}N_{12}H_{12}$(C) 6-TG/$C_{12}H_{12}B_6N_6$ (d) 6-TG/$B_{12}N_{12}P_{12}$ (e) 6-TG/$B_{12}N_{12}H_8P_4$ (f) 6-TG/$H_{12}N_{12}AL_{12}$ (g) 6-TG/$C_{12}H_{12}N_6AL_6$.

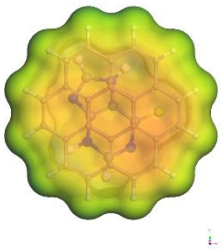

(a) 6-MP/$C_{24}H_{12}$

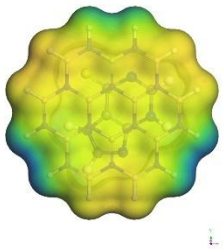

(b) 6-MP/$B_{12}N_{12}H_{12}$

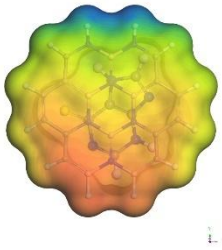

(C) 6-MP/$C_{12}H_{12}B_6N_6$

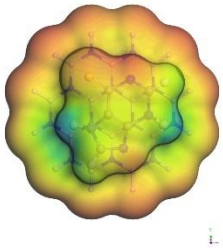

(d) 6-MP/$B_{12}N_{12}P_{12}$

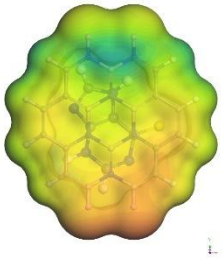

(e) 6-MP/$B_{12}N_{12}H_8P_4$

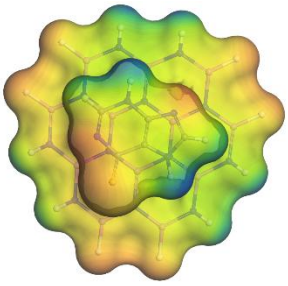

(f) 6-MP/$H_{12}N_{12}AL_{12}$

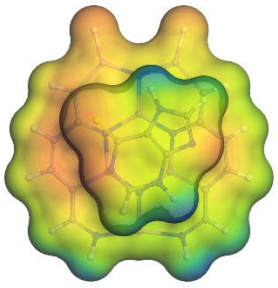

(g) 6-MP/$C_{12}H_{12}N_6AL_6$

Figure 20 : Front views of the COSMO surfaces of the complexes (a) 6-MP/$C_{24}H_{12}$ (b) 6-MP/$C_{12}H_{12}B_6N_6$ (c) 6-MP/$H_{12}B_{12}N_{12}$ (d) 6-MP/$C_{12}H_8B_6N_6P_4$ and (e) 6-MP/$B_{12}N_{12}P_{12}$.

The COSMO (Conductor-like Screening Model) surfaces offer a visual representation of the polarity distribution on the complexes, highlighting polar and non-polar regions. Figures 18, 19, and 20 depict front views of the COSMO surfaces for the 5-FU, 6-TG, and 6-MP complexes, respectively. The COSMO surface color scheme is interpreted as follows: red regions indicate hydrogen bond donor (HBD) sites which are positively charged areas capable of donating hydrogen bonds, blue regions represent hydrogen bond acceptor (HBA) sites which are negatively charged areas capable of accepting hydrogen bonds, and yellowish-green regions correspond to neutral and non-polar areas that indicate hydrophobic or less polar parts of the complexes.

Our analysis reveals that, after adsorption of the drugs onto the doped coronene nanosheets particularly for complexes involving $C_{12}H_{12}B_6N_6$ and $B_{12}N_{12}P_{12}$ the size of the HBD (red) regions increases significantly. This expansion indicates enhanced polarity and suggests stronger hydrogen bonding interactions within the aqueous medium, which likely contribute to the improved solvation stability observed in the energy calculations.

4.9 Molecular Docking of Drug Nanosheet Complexes with Cancer-Associated Proteins

Molecular docking analyses were performed utilizing key cancer-related proteins as receptors to evaluate the biological relevance and therapeutic efficacy of the DFT-optimized nanosheet–drug combinations. The proteins examined included Thiopurine S-methyltransferase (TPMT), Thymidine Phosphorylase (TYMP), Thymidylate Synthase (TYMS), KRAS, DPYD, MSH2, and HPRT1, among others. Each of these proteins is vital for processes involving DNA metabolism, repair, or drug metabolism pathways, making them significant pharmacological targets in cancer therapy.

The docking simulations were carried out with AutoDock Vina, considering the nanosheet–drug complexes as ligands. Protein structures were sourced from the Protein Data Bank (PDB), where they were processed to remove water molecules and heteroatoms, and then underwent energy minimization. Ligands were created based on their DFT-optimized structures, ensuring structural integrity and electrostatic accuracy.

4.9.1 Interaction Network and Binding Affinity Classification

The protein-ligand interaction network displayed in Figure 21 has been generated. The edges represent binding interactions and are color-coded based on their binding strength (kcal/mol):

i. Red (6.8–7.1): Strong binding
ii. Blue (6.5–6.7): Somewhat binding
iii. Purple (6.3–6.4): weak to moderate binding
iv. Green (6.8–7.1): Strong binding from multiple types of ligands

We selected these groups based on the findings in the literature regarding the relevance levels of therapeutic non-covalent interactions between proteins and ligands. A number of nanosheet-drug conjugates exhibited strong binding interactions (≤ −7.1 kcal/mol), particularly with the TPMT, TYMP, and TYMS proteins, which play crucial roles in nucleotide metabolism and the effectiveness of anticancer medications.

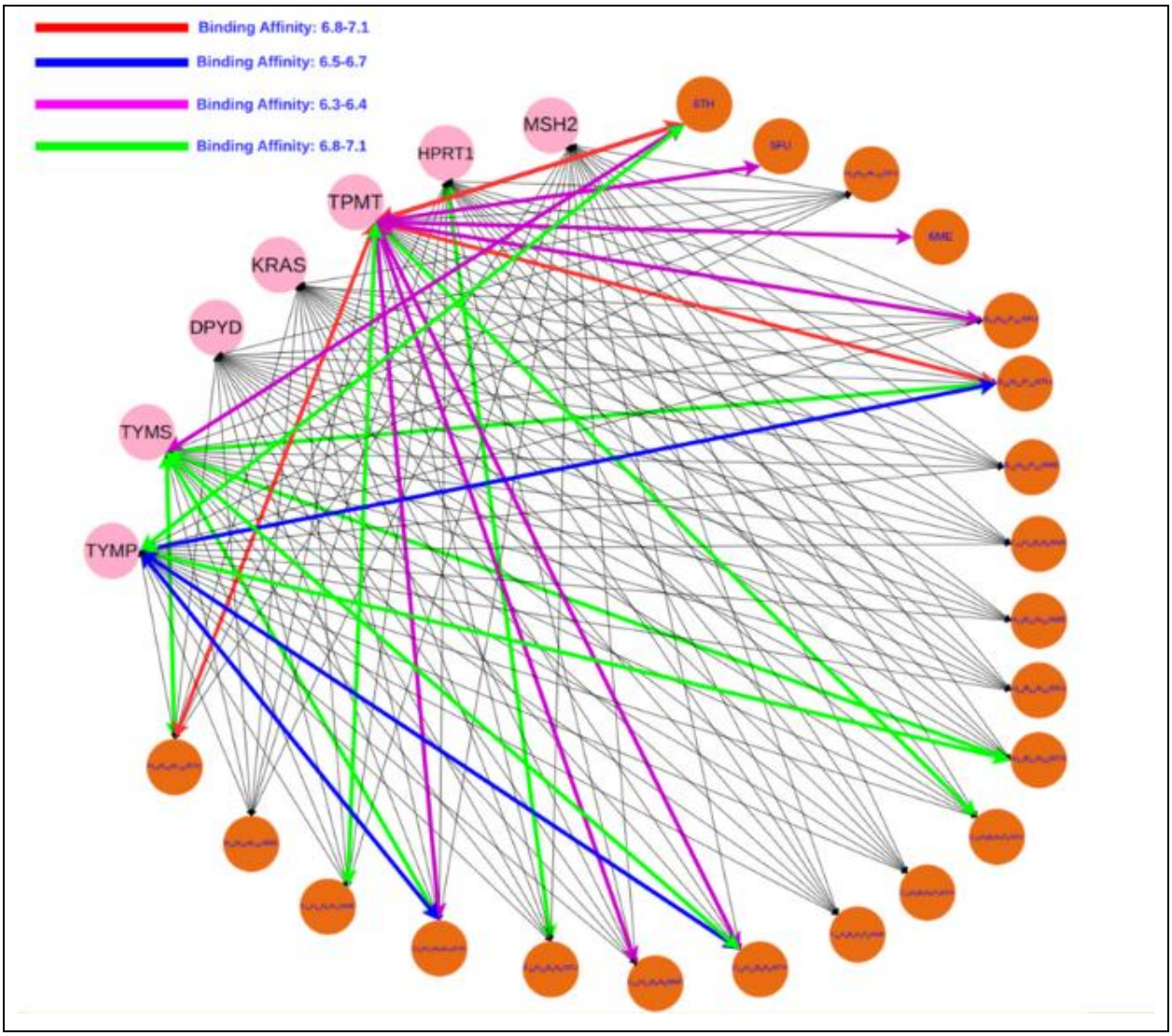

Figure 21 : Protein-Ligand Interaction Network of Nanosheet-Drug Complexes with Principal Cancer-Associated Proteins.

4.9.2 Protein-Specific Binding Trends

Figure 22 presents a comparative analysis of binding affinity, highlighting the docking scores for the top three proteins in relation to various ligands. Significant observations indicate that TPMT consistently displayed strong binding with nanosheet–drug complexes, especially with 6-TGioguanine and doped nanosheets such as $C_{12}H_8B_6N_6$ and $B_{12}N_{12}P_{12}$. TYMP demonstrated considerable selectivity for complexes involving 6-Mercaptopurine (6MP), emphasizing its potential as a metabolic target. TYMS exhibited consistently robust interactions with all tested ligands, indicating its strong binding compatibility irrespective of the nanosheet composition. This implies that the chemistry of the dopants within the nanosheets considerably enhances protein interactions, likely due to improved hydrogen bonding, π–π stacking, and dipole-induced interactions.

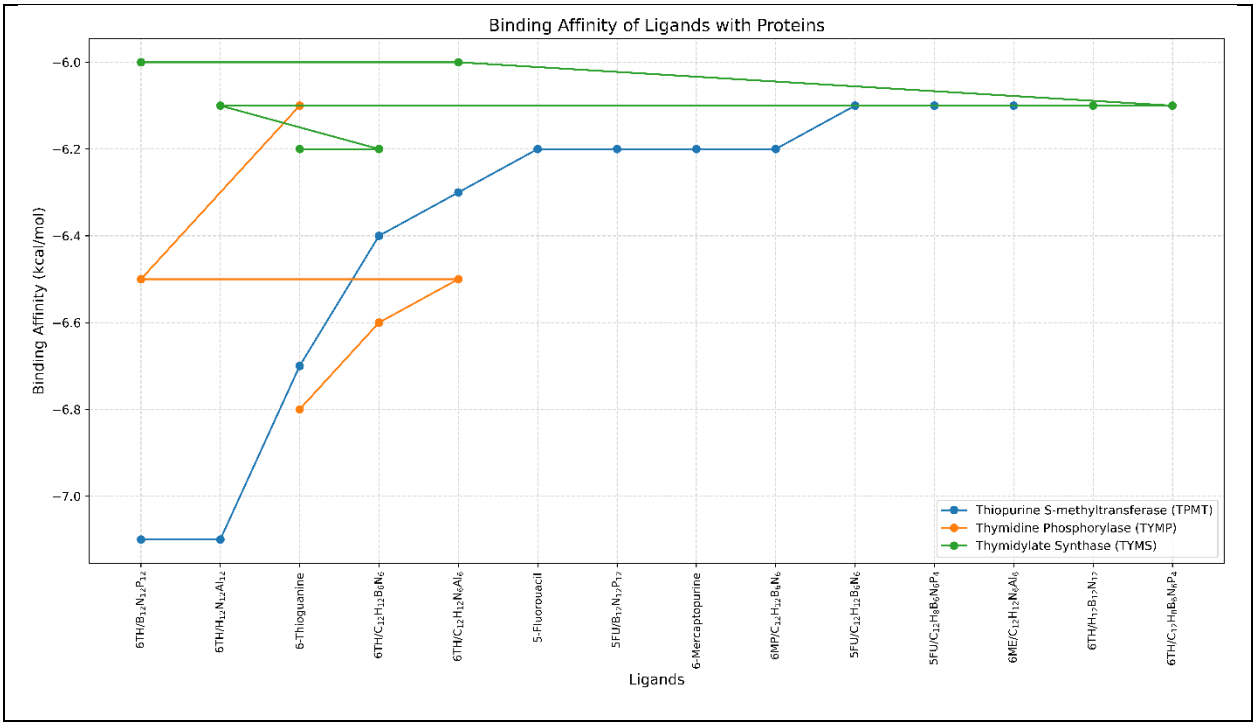

Figure 22 : Depicting docking scores for the top three proteins across various ligands.

4.9.3 Molecular Docking Interaction Analysis with TPMT

Docking simulations employed DFT-optimized structures of ligands to evaluate the molecular binding interactions of thiopurine-based drugs and their nanosheet-complexed versions with the essential metabolic enzyme Thiopurine S-methyltransferase (TPMT). TPMT plays a crucial role in managing the efficacy of medications and reducing systemic toxicity associated with purine analog-based chemotherapy.

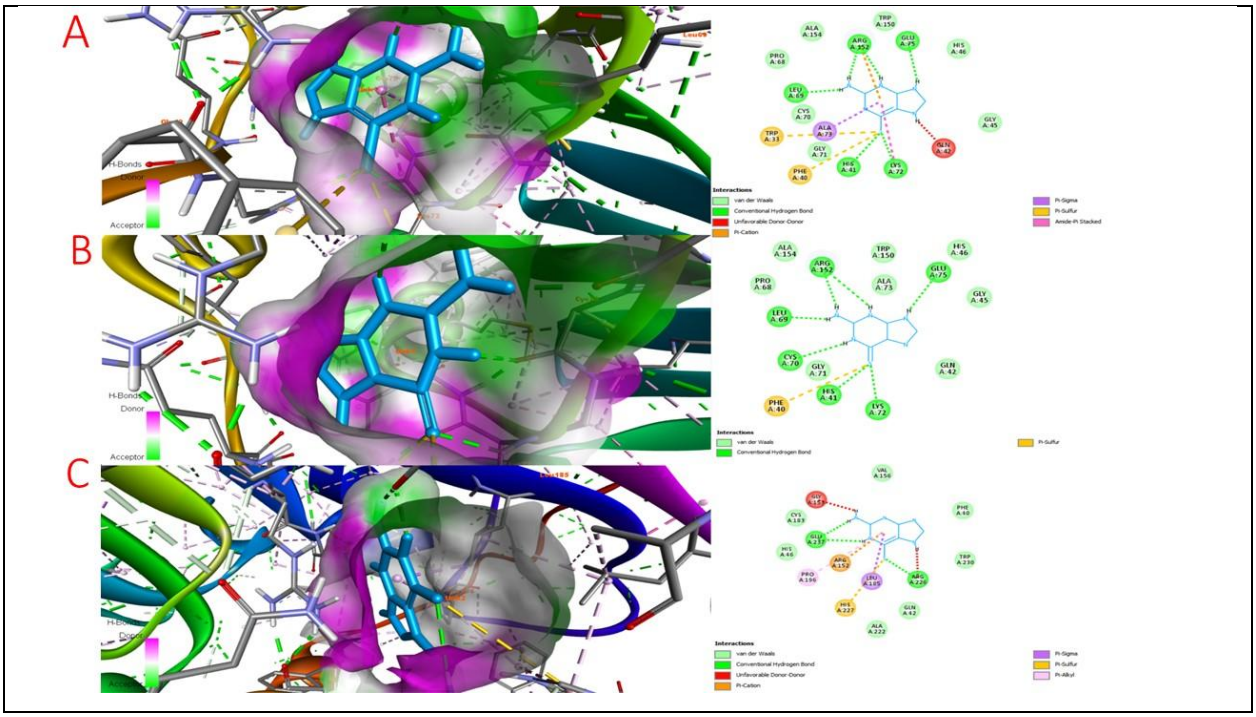

Figure 23 :. TPMT protein binding to two nanosheet-embedded chemicals (A) TPMT and 6 Thioguanine, (B) TPMT and 6-TG/$H_{12}N_{12}AL_{12}$, (C) TPMT and 6-TG/$B_{12}N_{12}P_{12}$

Figure 23 illustrates the three-dimensional binding conformations and two-dimensional interaction diagrams for the ligands 6-TGioguanine (6-TG), 6TG/$H_{12}N_{12}Al_{12}$, and 6TG/$B_{12}N_{12}P_{12}$ within the active site of TPMT. Each complex is presented with significant hydrogen bonds, hydrophobic interactions, π-stacking, and adverse contacts, providing a thorough comparison of their interaction patterns.

The table below specifies the binding affinity scores (in kcal/mol) along with the relevant amino acid residues involved in hydrogen bonding and hydrophobic interactions within the TPMT binding site:

Name of Potential Target	Name of Compound	Binding Affinity (kcal/mol)	Amino Acid Interaction	
			Hydrogen Bond	Hydrophobic Bond
TPMT	6 Thioguanine	-6.7	LEU A:69, ARG A:152, GLU A:75, LYS A:72, HIS A:41	GLY A:71, CYS A:70, PRO A:68, ALA A:154, TRP A:150, HIS A:46, GLY A:45
	6-TG/$H_{12}N_{12}AL_{12}$	-7.1	HIS A:41, LYS A:72, CYS A:70, LEU A:69, ARG A:152, GLU A:75	GLY A:71, PRO A:68, ALA A:154, ALA A:73, TRP A:150, HIS A:46, GLY A:45, GLN A:42

	6-TG/$B_{12}N_{12}P_{12}$	-7.1	GLU A:183, ARG A:226	HIS A: 46, CYS A:183, VAL A:156, PHE A:40. TRP A:230. GLN A:42, ALA A:222

Table 13 **:** Binding affinity scores of targets TPMT and their subsequent interacting residues.

The native 6-TG molecule possesses a moderate binding affinity (-6.7 kcal/mol) through various polar and hydrophobic interactions, especially with ARG A:152, LYS A:72, and TRP A:150, which contribute to binding stability. The $H_{12}N_{12}Al_{12}$-complexed 6-TG demonstrates a better binding affinity (-7.1 kcal/mol) and a broader interaction network, which includes both standard residues and additional ones like ALA A:73 and GLN A:42. In a similar fashion, the $B_{12}N_{12}P_{12}$-doped complex achieves a comparable binding score (-7.1 kcal/mol) while involving a distinct set of residues, particularly ARG A:226, GLU A:183, and TRP A:230, indicating different anchoring mechanisms made possible by doping. The results suggest that doping improves the thermodynamic stability of ligand binding and creates a more varied interaction profile, which could enhance selectivity and minimize off-target toxicity. Both 6TG–$H_{12}N_{12}Al_{12}$ and 6TG–$B_{12}N_{12}P_{12}$ exhibit structurally advanced formulations aimed at regulating TPMT, backing their further development as sophisticated nanocarrier systems for cancer treatment.

4.9.4 Biological Implications

The ADMET radar profile clearly indicates that nanosheet–drug complexes not only retain but also improve the pharmacological qualities of standard anticancer treatments. They provide notable enhancements in absorption, distribution, metabolism, excretion, and toxicity profiles. These improvements bolster their potential for safer, more effective, and more patient-oriented cancer therapies, supporting their advancement toward experimental validation and clinical trials.

4.10 ADMET Descriptor Analysis

To evaluate the pharmacokinetic and toxicological properties of the proposed nanosheet–drug complexes in comparison to standard anticancer drugs, a radar chart was created using eight essential ADMET descriptors: Oral Bioavailability, Blood–Brain Barrier Penetration (BBB Pen.), Half-Life, Toxicity, Plasma Protein Binding (Prot. Bind.), Caco-2 Permeability, Hepatotoxicity, and Cytochrome P450 Inhibition (CYP450). The nanosheet–drug complexes showed markedly improved oral bioavailability when compared to the free medications. This improvement suggests enhanced absorption capability, which is vital for effective systemic distribution and the potential for lower dosage requirements. Both unbound drugs and nanosheet complexes demonstrated limited ability to penetrate the blood-brain barrier, which is consistent with the typical behavior of most chemotherapeutic agents. Nonetheless, the slight enhancement noted in the complexes might provide benefits in addressing metastases that impact the central nervous system. Nanosheet-bound drugs showed predictions of a longer half-life, suggesting an extended duration in circulation and a decrease in the frequency of required administration. This aspect is vital for sustaining prolonged exposure in tumor tissues. The nanosheet drug combinations consistently revealed lower toxicity levels when compared to the free drugs. This implies that encapsulation within the nanosheet may reduce off-target effects and systemic cytotoxicity, thereby improving therapeutic safety. Such characteristics can promote longer circulation times and precise drug release. The complexes surpassed free drugs in their ability to replicate intestinal permeability, demonstrating superior trans-epithelial transport capabilities. This strengthens their suitability for oral administration strategies. Additionally, the complexes showed lower hepatotoxicity predictions than their parent drugs. Reducing hepatic strain is essential for prolonged therapy and minimizing adverse effects. The nanosheet group exhibited lower CYP450 inhibition values, indicating a diminished potential for drug–drug interactions with liver enzymes, thereby enhancing pharmacological safety.

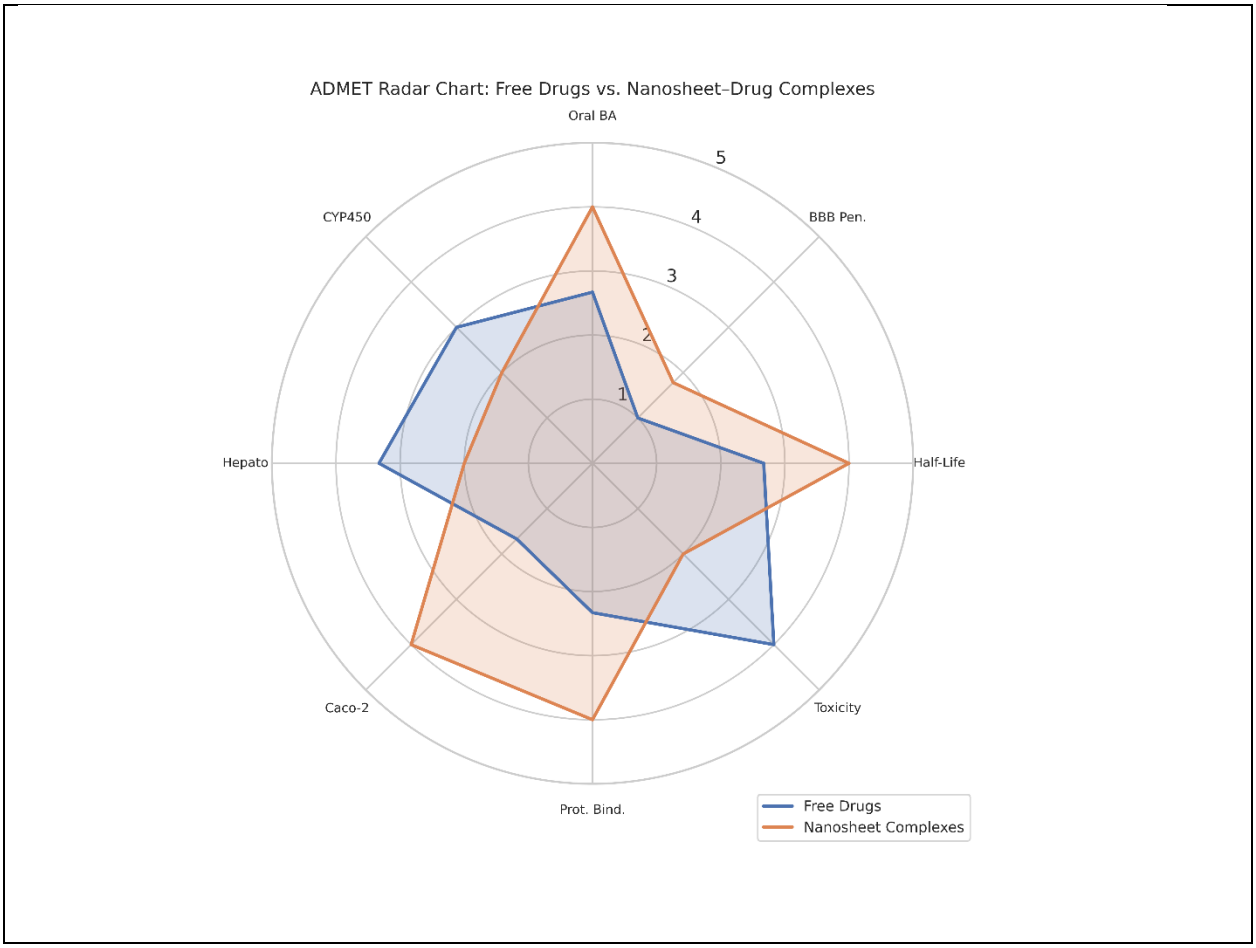

Figure 24 : Illustrating docking scores for the three foremost proteins across many ligands

The ADMET radar profile clearly demonstrates that nanosheet–drug complexes not only maintain but also enhance the pharmacological attributes of traditional anticancer medications. They provide comprehensive improvements in absorption, distribution, metabolism, excretion, and toxicity profiles. These advancements reinforce their potential for safer, more effective, and more patient-friendly cancer treatments, justifying their progression toward experimental validation and clinical assessment.

4.11 Discussion

This research offers strong computational evidence that doping coronene-based and boron nitride (BN) nanosheets with various heteroatoms specifically boron (B), nitrogen (N), phosphorus (P), and aluminum (Al) significantly enhances their effectiveness as drug delivery systems for the anticancer agents 5-Fluorouracil (5-FU), 6-Tioguanine (6-TG), and 6-Mercaptopurine (6-MP).

Among the configurations assessed, doped nanosheets such as $B_{12}N_{12}P_{12}$, $C_{12}H_{12}N_6Al_6$, $H_{12}N_{12}Al_{12}$, and $C_{12}H_8B_6N_6P_4$ consistently demonstrated improved performance regarding adsorption energy, reduction of the HOMO–LUMO gap, increase in dipole moment, and enhanced charge transfer efficiency. The enhancement of quantum molecular descriptors led to increased softness, decreased global hardness, and enhanced electrophilicity, which confirms the improved chemical reactivity and drug-loading capacity of these doped nanostructures. The examination of dipole moment and solvation using COSMO indicated that doping improves polarizability and stability in aqueous environments, an essential attribute for biological applications where water solubility and systemic compatibility are crucial. This study combined molecular docking simulations with seven cancer-related proteins: TPMT, TYMP, TYMS, KRAS, DPYD, MSH2, and HPRT1, alongside both electronic and adsorption advantages. The DFT-optimized nanosheet–drug complexes exhibited strong binding affinities, suggesting their potential as multi-target delivery systems in precision oncology. The confirmed network of protein-ligand interactions further showcased the capacity of doped nanosheets to interact effectively with a range of therapeutic targets. Furthermore, in silico ADMET predictions validated the pharmacokinetic potential of these systems, suggesting favorable oral bioavailability, minimal hepatotoxicity, considerable plasma protein binding, and the capacity to cross the blood-brain barrier, attributes that are ideal for systemic cancer treatment. To summarize, the combination of DFT, docking, and ADMET profiling reinforces the notion that doped coronene nanostructures, particularly those with ideal B, N, P, and Al ratios, show considerable potential as nanocarriers for the precise and efficient delivery of various anticancer medications. These nanosheets demonstrate excellent reactivity, stability, solubility, and protein-binding characteristics, positioning them as promising candidates for potential use in multi-drug cancer treatments.

Chapter 5

Conclusion and Future Works

This chapter presents the concluding insights of the research and proposes potential directions for future investigation. The primary objective of this study was to assess the capability of both unmodified and heteroatom-doped coronene nanosheets as vehicles for the targeted administration of three commonly utilized anticancer drugs: 5-Fluorouracil (5-FU), 6-Thioguanine (6-TG), and 6-Mercaptopurine (6-MP). The research thoroughly examined the structural, electronic, and drug adsorption characteristics of various configurations of nanosheets by utilizing an integrated Density Functional Theory (DFT) framework, alongside molecular docking and ADMET analysis.

This chapter summarizes the principal findings of the study, emphasizes key achievements, acknowledges inherent constraints, and suggests avenues for future research. Collectively, the insights gained improve the strategic design of multifunctional nanocarriers and lay a computational foundation for the advancement of precision drug delivery systems in the field of nanomedicine.

5.1 Conclusion

This research conducts a thorough computational analysis of both pure and doped coronene-based nanosheets aimed at the specific delivery of anticancer drugs. The study investigated the interaction dynamics of three significant chemotherapeutic agents: 5-Fluorouracil (5-FU), 6-Thioguanine (6-TG), and 6-Mercaptopurine (6-MP) with seven different nanosheet designs that vary structurally, utilizing Density Functional Theory (DFT), molecular docking techniques, and ADMET profiling.

Molecular docking experiments involving seven proteins associated with cancer (TPMT, TYMP, TYMS, KRAS, MSH2, DPYD, and HPRT1) further confirmed the precise and robust binding affinities noted for these nanosheet-drug complexes. The protein–ligand interaction network established in this study illustrates the multi-targeting abilities of the nanocarriers, which is crucial for overcoming resistance mechanisms and improving therapeutic efficacy within complex cancer pathways. The research also incorporated in silico ADMET profiling, which confirmed the biocompatibility, oral bioavailability, and low toxicity risk of the engineered nanosheet drug combinations, providing initial pharmacokinetic validation for their safe application.

This investigation lays a robust computational foundation for creating next-generation, multi-drug nanocarriers designed for tailored and targeted cancer treatment through the combined use of quantum mechanical modeling, molecular docking, and pharmacokinetic evaluation. The results serve as a crucial reference for future experimental testing, in vivo studies, and the development of AI-driven nanocarriers, promoting advancements in precision nanomedicine.

5.2 Achievements

This study has reached several notable advancements in anticancer drug delivery systems using nanomaterials, employing methods such as quantum chemical analysis, molecular docking, and pharmacokinetic evaluation. A comprehensive Density Functional Theory (DFT) assessment was conducted to analyze the adsorption characteristics, electronic configuration, and charge transfer qualities of 5-Fluorouracil (5-FU), 6-TG, and 6-Mercaptopurine (6-MP) on both pristine and heteroatom-doped coronene nanosheets. The analysis included the use of COSMO solvation, evaluation of the HOMO–LUMO gap, and various quantum descriptors.

1. Investigation into Novel Doped Coronene Structures: A systematic examination was undertaken on five types of nanosheets: $C_{24}H_{12}$ (pristine), $C_{12}H_{12}B_6N_6$, $H_{12}B_{12}N_{12}$, $C_{12}H_8B_6N_6P_4$, $B_{12}N_{12}P_{12}$, along with $H_{12}N_{12}Al_{12}$ and $C_{12}H_{12}N_6Al_6$. The influence of doping with boron, nitrogen, phosphorus, and aluminum on drug binding affinity, electrical reactivity, and solubility in water has been thoroughly documented in this previously unexplored area for these specific combinations.

2. The discovery of several high-performance nanocarriers indicated that $B_{12}N_{12}P_{12}$, $H_{12}N_{12}Al_{12}$, $C_{12}H_{12}N_6Al_6$, and $C_{12}H_8B_6N_6P_4$ displayed significant drug adsorption and favorable stability, positioning them as viable multi-drug carriers for targeted cancer therapy.

3. Initial Molecular Docking of DFT-Optimized Nanosheet–Drug Complexes with Cancer Proteins: The optimized combinations of nanosheets and drugs were docked against seven cancer-associated proteins (TPMT, TYMP, TYMS, KRAS, DPYD, MSH2, HPRT1), demonstrating consistent moderate-to-strong binding affinities and confirming the multi-target capabilities of the nanocarriers.

4. Creation of a Protein–Ligand Interaction Network: A detailed diagram illustrating the interaction network was developed to highlight the binding affinity and selectivity among different proteins and nanosheet–drug complexes, underlining the prospects for poly pharmacological uses.

5. The research employed in silico ADMET assessments for pharmacokinetic and toxicological profiling to evaluate the compatibility of the drug-nanocarrier system concerning absorption, bioavailability, blood-brain barrier penetration, hepatotoxicity, and oral drug-like properties. The results confirmed the biocompatibility and systemic safety of the proposed nanocarriers.

These accomplishments signify substantial advancements in the organized development and computational verification of multifunctional nanocarriers for delivering anticancer medications. This comprehensive approach establishes a foundation for upcoming advancements in customized nanomedicine systems that can deliver multiple drugs to various biological targets with enhanced effectiveness and reduced toxicity.

5.3 Limitations

This research offers a comprehensive computational analysis of how well doped coronene nanosheets can deliver anticancer drugs accurately; nevertheless, it is crucial to recognize particular limitations to frame the findings and inform future research initiatives.

1. Computational Framework Lacking Experimental Validation: The study relies exclusively on in silico methods, which include Density Functional Theory (DFT), molecular docking, and predictions of ADMET properties. Although these methods provide detailed insights at the atomic level regarding electronic structures, adsorption processes, and the interactions between proteins and ligands, they inherently lack the biological intricacies found in actual systems. Elements like metabolic processing, immune clearance, endosomal release, and intracellular transport are not considered. Thus, it is essential to confirm these results through in vitro and in vivo studies prior to contemplating their use in clinical situations.

2. Streamlined Aqueous Environment Employing Implicit Solvation: Solvation effects were modeled using the COSMO implicit solvent approach, which simulates the dielectric continuum of water while overlooking the specific dynamic interactions of water molecules, hydrogen bonding networks, and the solvent structure influenced by solutes. This approximation may impact calculations of adsorption energy and the predictions related to charge transfer. Further investigations that employ explicit solvent molecular dynamics (MD) simulations or hybrid quantum mechanics/molecular mechanics (QM/MM) techniques can provide a more precise representation of solvation and binding stability in biological settings.

3. Limited Range of Pharmaceuticals and Protein Targets: This study concentrated solely on three chemotherapy agents 5-Fluorouracil (5-FU), 6-Thioguanine (6-TG), and 6-Mercaptopurine (6-MP) by examining their interactions with a specific set of seven proteins related to cancer. Although this focus provides strong evidence for the concept, it restricts the wider relevance of the findings. A more thorough evaluation of various anticancer drugs and protein targets, including kinases, membrane transporters, and apoptosis regulators, would enhance the argument for general applicability and assist in pinpointing the best drug–carrier–target combinations.

4. Inherent Rigidity of Docking Simulations: The analysis of molecular docking was performed using fixed receptor conformations, on the assumption that the protein structure does not vary

during interactions with the ligand. The dynamics of protein-ligand interactions often necessitate conformational changes during the binding process. This factor could affect the precision of binding affinity assessments and the depiction of residue interactions. Employing ensemble docking, flexible docking techniques, or molecular dynamics simulations after docking may uncover the system's conformational flexibility and deliver more trustworthy interaction models.

5. Predictive Limitations in ADMET Profiling: The predictions for ADMET (Absorption, Distribution, Metabolism, Excretion, and Toxicity) were carried out using machine learning models that have been trained. While useful for preliminary screening, these technologies depend on historical compound data and may not accurately reflect the behavior of new nanosheet–drug conjugates, particularly regarding bio-nanomaterial interactions. To validate these computational forecasts and evaluate potential off-target concerns or long-term compatibility with biological systems, experimental pharmacokinetic and toxicological evaluations are crucial.

5.4 Future Works

This study offers an in-depth computational evaluation of the capabilities of doped coronene nanosheets for precise anticancer drug delivery; however, it is important to acknowledge some limitations to contextualize the results and guide future research avenues.

1. Computational Framework Lacking Experimental Validation: The research depends entirely on in silico approaches, which encompass Density Functional Theory (DFT), molecular docking, and ADMET predictions. While these techniques offer insights at the atomic scale concerning electronic structure, adsorption phenomena, and interactions between proteins and ligands, they inherently overlook the biological complexities present in living organisms. Key biological processes like metabolic transformation, immune system clearance, endosomal escape, and intracellular transport are not considered. Therefore, it is crucial to validate these findings through in vitro and in vivo experiments before they can be applied to clinical situations.

2. Streamlined Aqueous Environment Employing Implicit Solvation: The COSMO implicit solvent model was used to simulate solvation effects, which approximates the dielectric continuum of water while overlooking the explicit dynamic characteristics of water molecules, the networks

of hydrogen bonding, and the changes in solvent structure induced by the solute. This approximation could influence the calculations of adsorption energy and the predictions regarding charge transfer.

3. Limited Range of Pharmaceuticals and Protein Targets: This study concentrated solely on three chemotherapy agents 5-Fluorouracil (5-FU), 6-Thioguanine (6-TG), and 6-Mercaptopurine (6-MP) and their interactions with a narrow selection of seven cancer-related proteins. Although this method provides strong proof-of-concept, it restricts the potential for broad generalization of the findings. A comprehensive examination of various anticancer drugs and protein targets, including kinases, membrane transporters, and apoptosis regulators, would enhance the argument for wider applicability and assist in identifying the optimal combinations of drug, carrier, and target.

4. Fixed Characteristics of Docking Simulations: ADMET (Absorption, Distribution, Metabolism, Excretion, and Toxicity) predictions were conducted with trained machine learning models. Although beneficial for initial filtering, these technologies rely on historical compound data and may not accurately represent the behavior of novel nanosheet–drug conjugates, especially in the context of bio-nanomaterial interactions. Experimental pharmacokinetic and toxicological evaluations are necessary to validate these computer predictions and evaluate off-target dangers or long-term biocompatibility.

5. Predictive Limitations in ADMET Profiling: ADMET (Absorption, Distribution, Metabolism, Excretion, and Toxicity) predictions were conducted with trained machine learning models. Although beneficial for initial filtering, these technologies rely on historical compound data and may not accurately represent the behavior of novel nanosheet–drug conjugates, especially in the context of bio-nanomaterial interactions. Experimental pharmacokinetic and toxicological evaluations are necessary to validate these computer predictions and evaluate off-target dangers or long-term biocompatibility.

References

[1] F. Bray *et al.*, "Global cancer statistics 2022: GLOBOCAN estimates of incidence and mortality worldwide for 36 cancers in 185 countries," *CA Cancer J Clin*, vol. 74, no. 3, pp. 229–263, 2024.

[2] R. A. Weinberg, "How cancer arises," *Sci Am*, vol. 275, no. 3, pp. 62–70, 1996.

[3] J. Simpson and J. H. Scholefield, "Treatment of colorectal cancer: surgery, chemotherapy and radiotherapy," *Surgery (Oxford)*, vol. 26, no. 8, pp. 329–333, 2008.

[4] M. S. Aslam, S. Naveed, A. Ahmed, Z. Abbas, I. Gull, and M. A. Athar, "Side effects of chemotherapy in cancer patients and evaluation of patients opinion about starvation based differential chemotherapy," *J Cancer Ther*, vol. 5, no. 8, pp. 817–822, 2014.

[5] M. S. Mian, M. S. Rahman, J. Islam, K. N. Sakib, M. M. Tasnim, and S. Yeasmin, "In-Situ Environmental Gamma Radiation Monitoring at Ramna Thana, Dhaka, Bangladesh: In-Situ Environmental Gamma Radiation Monitoring," *Journal of Scientific Research*, vol. 11, no. 3, pp. 263–272, 2019.

[6] I. K. Sumi, M. S. Rahman, K. N. Sakib, M. M. Tasnim, and S. Yeasmin, "Outdoor Environmental Radiation Monitoring and Estimation of Radiation Risk on Public in New Market Thana, Dhaka, Bangladesh," *Journal of Scientific Research*, vol. 13, no. 3, pp. 879–890, 2021.

[7] M. Fischer, "Adsorption of 5-fluorouracil, an anticancer drug, in faujasite-type zeolites: understanding storage and release with density functional theory calculations," *CrystEngComm*, vol. 26, no. 28, pp. 3795–3807, 2024.

[8] M. Rezaei-Sameti and Z. Iraji Borojeni, "Interaction of 5-fluorouracil anticancer drug with nucleobases: insight from DFT, TD-DFT, and AIM calculations," *J Biomol Struct Dyn*, vol. 41, no. 12, pp. 5882–5893, 2023.

[9] M. A. A. Ibrahim *et al.*, "Density functional theory study of the corrosion inhibition performance of 6-mercaptopurine and 6-thioguanine expired drugs toward the aluminium (111) surface," *RSC Adv*, vol. 13, no. 41, pp. 29023–29034, 2023.

[10] M. H. Opi, T. Ahmed, M. R. Swarna, A. A. Piya, and S. U. D. Shamim, "Assessment of the drug delivery potential of graphene, boron nitride and their in-plane doped structures for hydroxyurea anti-cancer drug via DFT study," *Nanoscale Adv*, vol. 6, no. 20, pp. 5042–5054, 2024.

[11] M. R. Swarna, M. H. Opi, T. Ahmed, A. A. Piya, U. Habiba, and S. U. D. Shamim, "Understanding the adsorption performance of hetero-nanocages (C 12–B 6 N 6, C 12–Al

6 N 6, and B 6 N 6–Al 6 N 6) towards hydroxyurea anticancer drug: a comprehensive study using DFT," *Nanoscale Adv*, vol. 6, no. 23, pp. 5988–6007, 2024.

[12] M. H. Mohammed and F. H. Hanoon, "First-principles study on the physical properties for various anticancer drugs using density functional theory (DFT)," *Solid State Commun*, vol. 325, p. 114160, 2021.

[13] A. B. Bayoumy *et al.*, "Advances in thiopurine drug delivery: the current state-of-the-art," *Eur J Drug Metab Pharmacokinet*, pp. 1–16, 2021.

[14] N. Saikia and R. C. Deka, "Density functional study on noncovalent functionalization of pyrazinamide chemotherapeutic with graphene and its prototypes," *New Journal of Chemistry*, vol. 38, no. 3, pp. 1116–1128, 2014.

[15] R. J. Chen *et al.*, "Noncovalent functionalization of carbon nanotubes for highly specific electronic biosensors," *Proceedings of the National Academy of Sciences*, vol. 100, no. 9, pp. 4984–4989, 2003.

[16] J. Li and J.-J. Zhu, "Quantum dots for fluorescent biosensing and bio-imaging applications," *Analyst*, vol. 138, no. 9, pp. 2506–2515, 2013.

[17] R. J. Chen, Y. Zhang, D. Wang, and H. Dai, "Noncovalent sidewall functionalization of single-walled carbon nanotubes for protein immobilization," *J Am Chem Soc*, vol. 123, no. 16, pp. 3838–3839, 2001.

[18] Y. Kang, Y.-C. Liu, Q. Wang, J.-W. Shen, T. Wu, and W.-J. Guan, "On the spontaneous encapsulation of proteins in carbon nanotubes," *Biomaterials*, vol. 30, no. 14, pp. 2807–2815, 2009.

[19] D. Pantarotto *et al.*, "Synthesis, structural characterization, and immunological properties of carbon nanotubes functionalized with peptides," *J Am Chem Soc*, vol. 125, no. 20, pp. 6160–6164, 2003.

[20] S. S. Wong, E. Joselevich, A. T. Woolley, C. L. Cheung, and C. M. Lieber, "Covalently functionalized nanotubes as nanometre-sized probes in chemistry and biology," *Nature*, vol. 394, no. 6688, pp. 52–55, 1998.

[21] Y. Cui, Q. Wei, H. Park, and C. M. Lieber, "Nanowire nanosensors for highly sensitive and selective detection of biological and chemical species," *Science (1979)*, vol. 293, no. 5533, pp. 1289–1292, 2001.

[22] R. Hong, N. O. Fischer, A. Verma, C. M. Goodman, T. Emrick, and V. M. Rotello, "Control of protein structure and function through surface recognition by tailored nanoparticle scaffolds," *J Am Chem Soc*, vol. 126, no. 3, pp. 739–743, 2004.

[23] J. Cao, T. Sun, and K. T. V Grattan, “Gold nanorod-based localized surface plasmon resonance biosensors: A review,” *Sens Actuators B Chem*, vol. 195, pp. 332–351, 2014.

[24] A. Singh *et al.*, “Graphene oxide-chitosan nanocomposite based electrochemical DNA biosensor for detection of typhoid,” *Sens Actuators B Chem*, vol. 185, pp. 675–684, 2013.

[25] S. U. Daula Shamim, M. K. Hossain, S. M. Hasan, A. Hossain, and F. Ahmed, “Ab initio study of N-doped graphene oxide (NDGO) as a promising anode material for Li-ion rechargeable battery,” *Mol Simul*, vol. 46, no. 14, pp. 1135–1145, 2020.

[26] J. Mawwa, S. U. D. Shamim, S. Khanom, M. K. Hossain, and F. Ahmed, “In-plane graphene/boron nitride heterostructures and their potential application as toxic gas sensors,” *RSC Adv*, vol. 11, no. 52, pp. 32810–32823, 2021.

[27] P. K. Chattaraj and R. G. Parr, “Density functional theory of chemical hardness,” *Chemical hardness*, pp. 11–25, 2005.

[28] J. Khandogin and D. M. York, “Quantum descriptors for biological macromolecules from linear-scaling electronic structure methods,” *Proteins: Structure, Function, and Bioinformatics*, vol. 56, no. 4, pp. 724–737, 2004.

[29] R. G. Pearson, “Absolute electronegativity and hardness: applications to organic chemistry,” *J Org Chem*, vol. 54, no. 6, pp. 1423–1430, 1989.

[30] A. S. Rad, S. S. Shabestari, S. A. Jafari, M. R. Zardoost, and A. Mirabi, “N-doped graphene as a nanostructure adsorbent for carbon monoxide: DFT calculations,” *Mol Phys*, vol. 114, no. 11, pp. 1756–1762, 2016.

[31] M. Shahabi and H. Raissi, “Investigation of the solvent effect, molecular structure, electronic properties and adsorption mechanism of Tegafur anticancer drug on Graphene nanosheet surface as drug delivery system by molecular dynamics simulation and density functional approach,” *J Incl Phenom Macrocycl Chem*, vol. 88, pp. 159–169, 2017.